


RESEARCH

Open Access



Monitoring imatinib decreasing pericyte coverage and HIF-1 α level in a colorectal cancer model by an ultrahigh-field multiparametric MRI approach

Xinpeng Hu^{1†}, Kunlin Ye^{1†}, Shaowei Bo², Zeyu Xiao^{1,3}, Mengjie Ma⁴, Jinghua Pan⁵, Xing Zhong¹, Dong Zhang¹, Xukai Mo¹, Xiaojun Yu¹, Minfeng Chen^{6*}, Liangping Luo^{1,3*} and Changzheng Shi^{1,3*} 

Abstract

Background Excessive pericyte coverage promotes tumor growth, and a downregulation may solve this dilemma. Due to the double-edged sword role of vascular pericytes in tumor microenvironment (TME), indiscriminately decreasing pericyte coverage by imatinib causes poor treatment outcomes. Here, we optimized the use of imatinib in a colorectal cancer (CRC) model in high pericyte-coverage status, and revealed the value of multiparametric magnetic resonance imaging (mpMRI) at 9.4T in monitoring treatment-related changes in pericyte coverage and the TME.

Methods CRC xenograft models were evaluated by histological vascular characterizations and mpMRI. Mice with the highest pericyte coverage were treated with imatinib or saline; then, vascular characterizations, tumor apoptosis and HIF-1 α level were analyzed histologically, and alterations in the expression of Bcl-2/bax pathway were assessed through qPCR. The effects of imatinib were monitored by dynamic contrast-enhanced (DCE)-, diffusion-weighted imaging (DWI)- and amide proton transfer chemical exchange saturation transfer (APT CEST)-MRI at 9.4T.

Results The DCE- parameters provided a good histologic match the tumor vascular characterizations. In the high pericyte coverage status, imatinib exhibited significant tumor growth inhibition, necrosis increase and pericyte coverage downregulation, and these changes were accompanied by increased vessel permeability, decreased microvessel density (MVD), increased tumor apoptosis and altered gene expression of apoptosis-related Bcl-2/bax pathway. Strategically, a 4-day imatinib effectively decreased pericyte coverage and HIF-1 α level, and continuous treatment led to a less marked decrease in pericyte coverage and re-elevated HIF-1 α level. Correlation analysis confirmed the feasibility of using mpMRI parameters to monitor imatinib treatment, with DCE-derived V_e and k^{trans}

[†]Xinpeng Hu and Kunlin Ye contributed equally to this work.

*Correspondence:

Minfeng Chen
minfengchen@jnu.edu.cn
Liangping Luo
tluolp@jnu.edu.cn
Changzheng Shi
tsczc@jnu.edu.cn

Full list of author information is available at the end of the article



© The Author(s) 2024. **Open Access** This article is licensed under a Creative Commons Attribution-NonCommercial-NoDerivatives 4.0 International License, which permits any non-commercial use, sharing, distribution and reproduction in any medium or format, as long as you give appropriate credit to the original author(s) and the source, provide a link to the Creative Commons licence, and indicate if you modified the licensed material. You do not have permission under this licence to share adapted material derived from this article or parts of it. The images or other third party material in this article are included in the article's Creative Commons licence, unless indicated otherwise in a credit line to the material. If material is not included in the article's Creative Commons licence and your intended use is not permitted by statutory regulation or exceeds the permitted use, you will need to obtain permission directly from the copyright holder. To view a copy of this licence, visit <http://creativecommons.org/licenses/by-nc-nd/4.0/>.

being most correlated with pericyte coverage, V_e with vessel permeability, AUC with microvessel density (MVD), DWI-derived ADC with tumor apoptosis, and APT CEST-derived MTR_{asym} at 1 μT with HIF-1 α .

Conclusions These results provided an optimized imatinib regimen to achieve decreasing pericyte coverage and HIF-1 α level in the high pericyte-coverage CRC model, and offered an ultrahigh-field multiparametric MRI approach for monitoring pericyte coverage and dynamics response of the TME to treatment.

Keywords Imatinib, Pericyte coverage, TME, DCE-MRI, DWI, APT CEST

Introduction

Colorectal cancer (CRC) is an extremely challenging disease and pose a serious threat to human health, with an expected incidence of 153,020 cases and 52,550 deaths in 2023 [1]. To improve the prognosis of CRC patients, the National Comprehensive Cancer Network (NCCN) guidelines recommend the utilization of antiangiogenic drugs in advanced CRC [2, 3]. Notably, antiangiogenic drugs can turn off ‘angiogenic switches’ in a targeted manner to starve tumors while having minimal side effects [4–6]. Looking into tumor vasculature, pericytes are a cluster of mural cells covering vascular endothelial cells (ECs), participating in regulating vascular stabilization, angiogenesis, vascular permeability and blood flow [7–12]. Pericyte coverage, i.e., the proportion of pericytes to ECs, is a histological indicator of vascular structure and function [13]. Since the high expression of platelet-derived growth factor receptor beta (PDGFR β) in CRC pericytes rather than in tumor cells, and imatinib, a potent inhibitor of PDGFR- β , can tip off the PDGF-BB/PDGFR β pathway ‘switch’ and decrease pericyte coverage [14–17]. In clinical practice, imatinib has been used in the treatment of multiple malignancies, and its potential antiangiogenic properties make it worth exploring in CRC [18–20].

Recent studies have demonstrated that excessive pericyte coverage promotes tumor proliferation and progression through direct and indirect crosstalk between pericytes and the tumor microenvironment (TME). That is, Pericytes not only communicate directly with tumor cells but also promote tumor growth and progression by facilitating tumor angiogenesis, forming a pericyte-endothelial barrier to protect tumor cells, regulating proliferation, recruitment and function of immune cells [21–24]. Additionally, excessive pericyte coverage indicates poorer efficacy of antitumor therapies. Several studies have shown that residual pericytes lead to rapid revascularization of tumors and then restore blood flow after anti-VEGF drug withdrawal [25–30]. Targeting pericytes with pharmacological or genetic approaches can prolong the effects of anti-VEGF drugs by inhibiting tumor vessel regrowth [26–30]. Furthermore, a stable vasculature with high pericyte coverage acts as a hindrance to antitumor nanoparticles, whereas reduced pericyte coverage facilitates the passage of nanoparticles across vascular barriers

by increasing vascular permeability [31–33]. Moreover, high pericyte coverage and vascular stability are closely associated with accelerated tumor progression and poor prognosis in clinical trials, which indicates that down-regulating pericyte coverage by imatinib might inhibit tumor development in the presence of excessive pericyte coverage [34, 35]. However, low pericyte coverage indicates increased metastatic potential due to upregulation of hypoxia-induced hypoxia inducible factor-1 α (HIF-1 α) expression [17]. Targeting pericytes in the hypoxic TME accelerates tumor metastasis and leads to an unfavorable prognosis [36]. Taken together, these findings indicate that pericytes play the role of a double-edged sword in the TME; only rationally regulating pericyte coverage can exert antitumor effects, while inappropriate modulation of pericytes has the opposite effect. Thus, it is necessary to identify the relationship between imatinib-regulated pericyte coverage and TME indicators and optimize the use of imatinib. Myeloid cell leukemia-1 (Mcl-1) is a Bcl-2 family protein that suppresses apoptosis by interfering with mitochondrial activation [37]. As Mcl-1 is an important TME indicator, and its overexpression is associated with tumor progression and resistance to multiple antitumor drugs [38–41]. In addition, decreasing pericyte coverage by a PDGFR β inhibitor regulates Bcl-w in ECs, a component of the Bcl-2 pathway [42]. Unfortunately, the correlation between imatinib-regulated pericyte coverage and Mcl-1 expression remains unknown and needs to be investigated. Moreover, a noninvasive approach for longitudinal monitoring of pericyte coverage and the TME response, allowing for personalized adjustment of the treatment regimen as needed, is essential for the development of an effective imatinib treatment strategy. Hence, there is an urgent need to develop an appropriate method for monitoring the effect of imatinib on pericyte coverage and the TME.

As a noninvasive quantitative imaging tool, magnetic resonance imaging (MRI) provides macroscopic tumor insight into antiangiogenic therapies. Dynamic contrast-enhanced (DCE)-MRI holds significant value in evaluating changes in tumor vascular perfusion and permeability, as well as in predicting the efficacy of anti-VEGF drugs [43, 44]. Thus, DCE-MRI may be suitable for monitoring hemodynamic changes resulting from imatinib-mediated regulation of pericyte coverage, but

optimization and validation are required. For monitoring subtle changes in pericyte coverage and the TME during treatment by DCE-MRI, two technical obstacles need to be overcome: increasing the sensitivity of DCE-MRI for capturing vascular features and capturing TME features beyond the vasculature [43, 44]. Thus, we performed DCE-MRI at 9.4 Tesla (9.4T) to achieve optimal spatial resolution and sensitivity and monitored the heterogeneous TME through multiparametric MRI (mpMRI) [45–47]. During administration of imatinib treatment, the tumor cell response and tumor hypoxia also need to be monitored to obtain a global view of the TME. The apparent diffusion coefficient (ADC) value obtained by diffusion-weighted imaging (DWI) provides information on cellularity and indicates the tumor response to anti-tumor treatments [48–50]. For monitoring pH changes, Phosphorous-31 (^{31}P) Magnetic Resonance Spectroscopy (MRS) is a commonly used imaging technique, but it has inherent limitations, including a low resolution, low signal-to-noise ratio and long scan time [51, 52]. Amide proton transfer chemical exchange saturation transfer (APT CEST)-MRI is a novel molecular imaging technique that reflects the protein content and is sensitive to pH changes in tissues by detecting magnetization transfer from labeled amide protons (resonating at 3.5 ppm downfield from water) [53]. APT CEST-MRI offers high spatial resolution and high sensitivity to pH changes, making it an attractive method for monitoring hypoxia-induced acid–base imbalance [54–56].

Here, we developed an effective imatinib treatment strategy and adopted an ultrahigh-field mpMRI approach to monitor trends in pericyte coverage and the TME during treatment in a CRC model with high pericyte coverage. First, mice with the highest and lowest pericyte coverage of CRC were identified by immunofluorescence (IF) staining, and the IF data were found to match the DCE-MRI parametric values. Second, the antitumor response, histological changes in the vasculature and TME, and changes in associated pathways were evaluated to confirm the effectiveness of imatinib treatment. Third, a noninvasive evaluation approach involving DCE-, DWI- and APT CEST-MRI was established, and the feasibility of multiple parameters in monitoring pericyte coverage and the TME in response to treatment was confirmed. Finally, the correlation among the histological results and between the histological and imaging results was assessed, and the results indicated that the changes in histological indicators and imaging biomarkers were consistent. In conclusion, the application of imatinib in a CRC model with high pericyte coverage was optimized, and ultrahigh-field 9.4T mpMRI can be used to monitor local pericyte coverage and global changes in the TME to confirm therapeutic efficacy.

Materials and methods

Cell cultures

The HCT116, HT-29, RKO and SW480 human CRC cell lines were purchased from the American Type Culture Collection (ATCC, Manassas, Virginia). McCoy's 5a medium was used for HT-29 cells, and Dulbecco's modified Eagle's medium (DMEM) was used for HCT116, RKO and SW480 cells; both types of medium were supplemented with 10% FBS. The cells were cultured at 37 °C in a 5% CO_2 incubator.

Animal models

All animal experiments were conducted in accordance with procedures approved by the Laboratory Animal Ethics Committee of Jinan University (No. 20220304-47). A total of 70 male BALB/c nude mice (4–6 weeks old, body weight ~20 g) were purchased from Vital River Laboratory Animal Technology Co. Ltd. (Beijing, China) and maintained under specific pathogen-free conditions. To generate four types of CRC xenograft models, the mice were subcutaneously injected with 5×10^6 HCT116, HT-29, RKO, or SW480 cells into the right flank. After 14 days, tumors with a volume of approximately 200 mm^3 were harvested to ensure the presence of a highly developed vasculature for MRI. T2WI and DCE sequences were used to measure tumor volume and necrosis volume.

Drug treatment and study schedule

Sixty-two out of 70 mice that developed tumors were selected for the experiment. Figure 1 presents the design of the study in which 9.4T mpMRI and histological evaluation were performed during imatinib treatment. To identify mice with high and low pericyte coverage of CRC, the vascular characterizations of three mice each with the four CRC xenograft types were assessed by histological analysis (Fig. 1A). Five CRC model mice with high and low pericyte coverage were subjected to mpMRI (Fig. 1B). As shown in Fig. 1C, CRC model mice with high pericyte coverage were randomly divided into 2 groups ($n=20$ per group): the imatinib and control groups. Two weeks after implantation, mice in the imatinib group were intraperitoneally injected with imatinib mesylate (45 mg/kg, bid, TargetMol) for 10 days, and the control group was treated with an equal volume of 0.9% normal saline [57]. The vascular characterizations and TME indicators of 3 mice in the imatinib and control histology subgroups ($n=12$ per group) were histologically analyzed at baseline and on Day 4, Day 7 and Day 10. Mice in the imatinib and control MRI subgroups ($n=5$ per group) underwent MRI scans at each time point during treatment. On Day 10 of treatment, three mice from the imatinib and control groups were chosen for quantitative polymerase chain reaction (qPCR).

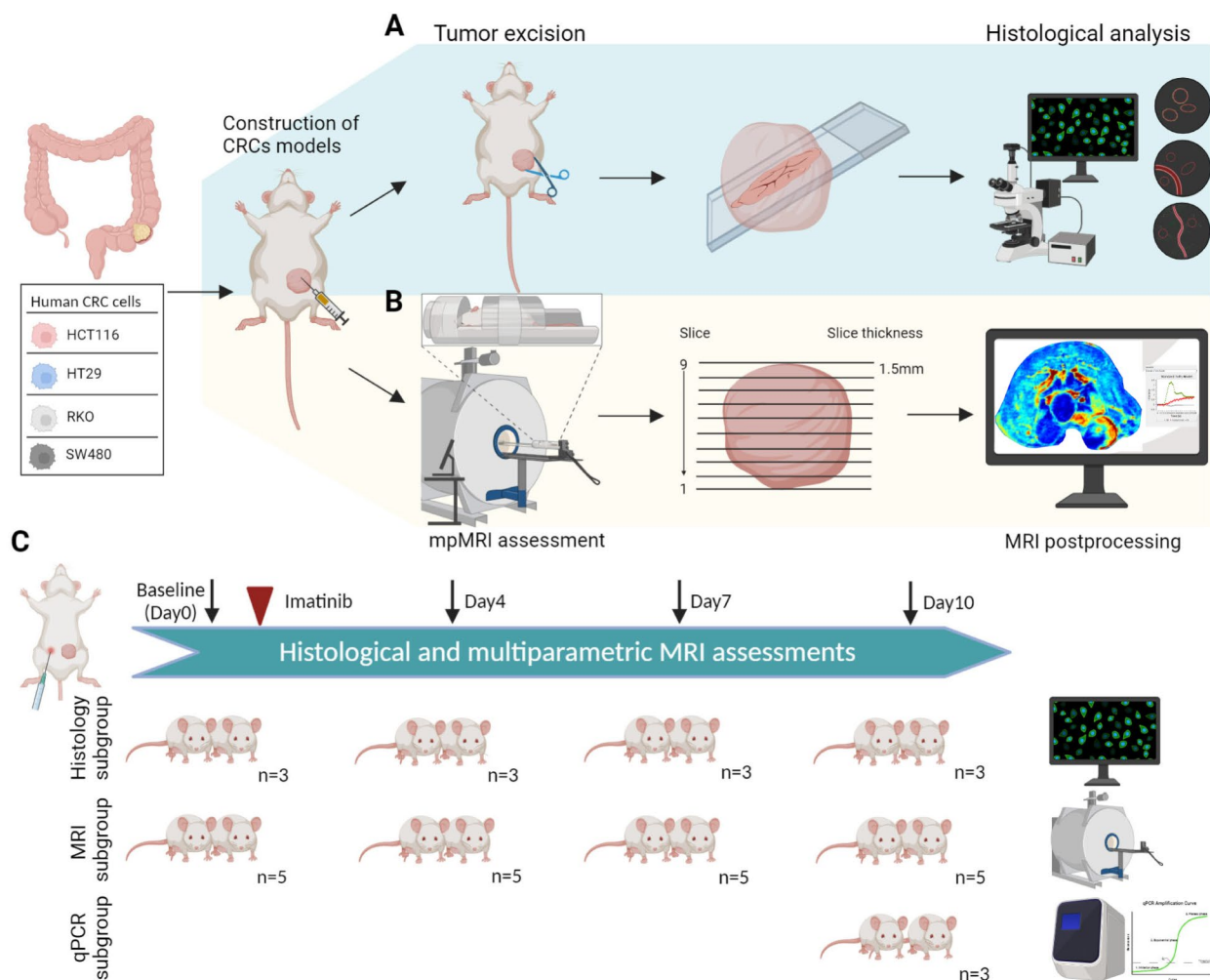


Fig. 1 9.4T mpMRI combined with histological techniques was used to monitor the TME during an imatinib treatment. **(A)** Three mice with the four CRC tumor types were used for histological analysis of vascular characteristics, and models with high and low pericyte coverage were selected. **(B)** Five mice with different CRC tumor types with high or low pericyte coverage were monitored by mpMRI. **(C)** CRC model mice with high pericyte coverage were treated with imatinib or saline and divided into histology, MRI, and qPCR subgroups. During the treatment, three mice in each group at each time point were sacrificed for histological analysis. Five mice in each group were used for the longitudinal mpMRI study. qPCR analysis was performed on three mice in the control and imatinib groups on Day 10. Figure 1 was drawn by Biorender

Histological analysis

There were a total of twenty-four mice in the histology subgroups. Three mice from the imatinib group and control group were sacrificed at baseline and on Day 4, Day 7 and Day 10 for histological analysis. Tumor tissues were routinely prepared for histological analysis through fixation, paraffin embedding and sectioning. H&E staining was performed according to standard procedures. For IF staining, tissue sections were subjected to antigen retrieval; then, nonspecific binding was blocked, followed by incubation with primary antibodies (diluted 1:200). The antibodies used included anti-Ki-67 (GB111141, Servicebio), anti-HIF-1 α (BF8002-50, Affinity), anti-Mcl-1 (GB11696, Servicebio), anti-CD31 (BG11063-1, Servicebio), anti- α -smooth muscle actin (α -SMA) (GB13044,

Servicebio), and anti-PDGFR β (bs-0232R, Bioss) antibodies. Subsequently, CY3- or FITC-conjugated secondary antibodies (diluted 1:300) were added to form immune complexes. TUNEL staining was performed using the FITC TUNEL Cell Apoptosis Detection Kit (G1501-50T, Servicebio) according to the manufacturer's instructions.

The vessel leakage assay was performed with frozen tissue sections. Thirty minutes before sacrifice, 200 μ L FITC-dextran (25 mg/mL, 40 kDa, Sigma-Aldrich) was intravenously injected into the tail vein of mice. Following removal of tumor tissue, fixation, dehydration, and permeabilization were carried out, followed by freezing in optimal cutting temperature (OCT) compound and sectioning. After blocking of nonspecific binding, the sections were sequentially incubated with an anti-CD31

antibody and fluorescent secondary antibody. Under a fluorescence microscope, three representative fields (at $\times 200$ magnification) of each section were selected for evaluation using ImageJ software (NIH).

MVD is the average vessel number in hot spot areas [58]. Pericyte coverage was calculated as the percentage of the pericyte marker⁺ area relative to the CD31⁺ area after exclusion of interstitial tissues and pericytes unrelated to the vasculature [13, 58]. Relative vessel permeability was calculated as the percentage of the FITC-dextran⁺ area relative to the CD31⁺ area [13, 59]. For the analysis of Ki-67, TUNEL, HIF-1 α , and Mcl-1 staining, at least 3 tumors and 3 random fields in each section were used. The percentage of positively stained cells relative to all tumor cells was calculated.

MRI protocol

All MRI scans were performed using a 9.4T MRI system (Bruker Biospec 94/30 Ettlingen, Germany) equipped with a dedicated mouse coil optimized for animal imaging. The mice were anesthetized with an intraperitoneal injection of 0.3% pentobarbital and imaged in the supine position. The scanning sequences included the following: T2WI (Turbo-RARE, repetition time (TR)/echo time (TE): 2000 ms/20 ms, number of averages: 2, field of view (FOV): 30×26 mm², matrix size: 256×196 , slice thickness: 1.5 mm), DWI-MRI (SE-EPI, TR/TE: 3200 ms/25.2 ms, b-values: 0 and 400 s/mm², number of averages: 1, FOV: 30×26 mm², matrix size: 128×128 , slice thickness: 1.5 mm), and DCE-MRI (FLASH, TR/TE: 30 ms/2 ms, flip angle: 20°, number of averages: 2, FOV: 30×26 mm², matrix size: 128×128 , slice thickness: 1.5 mm, 55 dynamics.) The contrast agent (Gadovist®, Bayer) was administered via tail vein injection, preceded by the acquisition of 15 baseline dynamics. For APT CEST-MRI data acquisition, long cw saturation pulses were applied for 3 s with $B_1 = 1$ μ T and $B_1 = 2$ μ T. The saturation pulses were applied at 65 offsets ranging from -6.4 to $+6.4$ ppm with a step size of 0.2 ppm and an additional offset of $+40$ ppm for a total of 68 offsets. Water saturation shift referencing (WASSR) images were collected to generate B0 maps using 31 offsets ranging from -1.5 to $+1.5$ ppm with a step size of 0.1 ppm and $B_1 = 0.5$ μ T. Each set of 68 offsets required a total time of 5 min and 40 s. The sequence parameters were as follows: TR/TE: 5000 ms/4.6 ms, number of averages: 1, FOV: 30×26 mm², matrix size: 64×64 , and slice thickness: 1.5 mm.

MRI data postprocessing

DWI-MRI images were processed by two experienced radiologists using a dedicated postprocessing workstation (360v1.1, Bruker). ADC values were calculated by fitting a single exponential to all b-values. ADC was calculated using Eq. (1).

$$\text{ADC} = [\ln(S_2/S_1)] / (b_1 - b_2) \quad (1)$$

where S_1 and S_2 represent the signal intensities from $b_1 = 400$ s/mm² and $b_2 = 0$ s/mm², respectively.

DCE-MRI data were analyzed using the software Medical Imaging Interaction Toolkit (MITK) Workbench [60]. After fitting the vascular input function (VIF), an extended Tofts mathematical model was used to calculate K^{trans} , V_e , K_{ep} , and area under the enhancement curve (AUC) (using all dynamic images) for the contrast agent [61–64]. $C(t)$ was calculated using Eq. (2).

$$C(t) = K^{\text{trans}} \cdot e^{-tK_{\text{ep}}} * C_a(t) \quad (2)$$

where “*” represents convolution, and $C(t)$ and $C_a(t)$ represent the concentration-time curves for the region of interest tissue and the arterial input, respectively. K_{ep} is equal to K^{trans}/V_e .

APT CEST-MRI images were B0-corrected using the WASSR method. Z-spectrum was generated by custom scripts written in MATLAB 2021b (MathWorks, Natick, Massachusetts) [53, 65] and fitted by the Lorentzian model [66]. $\text{MTR}_{\text{asym}(\Delta\omega)}$ is the signal in the z-spectrum at $\Delta\omega$ and was calculated using Eq. (3).

$$\text{MTR}_{\text{asym}(\Delta\omega)} = \frac{(S_{\text{sat}(-\Delta\omega)} - S_{\text{sat}(\Delta\omega)})}{S_0} \quad (3)$$

where $S_{\text{sat}(\Delta\omega)}$ and $S_{\text{sat}(-\Delta\omega)}$ represent the MRI signals at specific offset frequencies $\Delta\omega$ and $-\Delta\omega$ after RF irradiation, respectively, while S_0 represents the unsaturated signal. $\Delta\omega$ equals 3.5 ppm to achieve APT signal.

qPCR protocol

On Day 10, mice from the imatinib group and control group ($n=3$) were euthanized to excise tumor tissues. Total RNA was then extracted using an RNA extraction kit (Magen Biotech, Guangzhou, China). Then, the total RNA was reverse transcribed into cDNA using HIScriptQ Select RT SuperMix (Vazyme, Nanjing, China) according to the manufacturer’s protocol. qPCR was performed in a 20 μ L volume, including 10 μ L of SYBR Green PCR Master Mix, 2 μ L of diluted cDNA, 0.5 μ L of specific primers, and 7 μ L of ddH₂O. Three biological replicates were conducted for each gene, and the results are presented as the mean \pm standard deviation. The reaction protocol was as follows: incubation at 95 °C for 30 s; 40 cycles of denaturation at 95 °C for 10 s, annealing at 60 °C for 30 s, and extension at 72 °C for 20 s; and a final incubation at 4 °C for 5 min. The data were analyzed using the $2^{-\Delta\Delta C_t}$ method.

Statistical analysis

SPSS 24.0 software (IBM Corporation, Chicago, USA), GraphPad Prism 7.0 (GraphPad Software Inc., San Diego, USA) and R software were applied to perform statistical tests and generate dot-bar charts, line charts and correlation charts. All numerical results are presented as the mean \pm standard deviation. The normal distribution of the obtained data was assessed by the Kolmogorov-Smirnov test. For comparing quantitative histological and MRI data from the CRC models, one-way analysis of variance (ANOVA) with the least significant difference (LSD) test and Student's t test were applied. Student's t test was also used for comparisons of MRI and histological data between groups at the specific time point. One-way ANOVA was utilized for comparisons of MRI and histological data among different time points within groups. Pearson correlation analysis was used to analyze the correlation between mpMRI and histological data, as well as among histological data. $P < 0.05$ was considered to indicate statistical significance.

Results

Vascular characterization of CRC tumors

Due to a double-edged sword role of pericytes in the TME, imatinib treatment strategies can increase the effectiveness of antitumor therapies in the presence of excessive pericyte coverage, but inappropriate modulation of pericyte coverage has detrimental effects. Nevertheless, an effective imatinib regimen and a longitudinal monitoring technique for pericyte coverage are lacking. In this study, we employed mpMRI to monitor the effects of imatinib on vascular characterization and the TME in CRC with high pericyte coverage to determine for an optimized strategy. To generate tumor models with the highest level of pericyte coverage, subcutaneous tumors were generated in mice with four human CRC cell lines, and vascular characterization was conducted through IF analysis. Representative H&E-, CD31/PDGFR β -, CD31/ α -SMA-, CD31/dextran- and CD31-stained tumor tissue sections from the four model types are shown in Fig. 2A. HT-29 tumors had the highest PDGFR β ⁺ pericyte coverage, while HCT116 tumors displayed the lowest PDGFR β ⁺ pericyte coverage (Fig. 2B; Table 1). Similar distinctions in α -SMA⁺ pericyte coverage were observed between HT-29 and HCT116 tumors (Fig. 2C; Table 1). Compared to that in HT-29 tumors, PDGFR β ⁺ and α -SMA⁺ pericyte coverage in RKO and SW480 tumors was significantly lower (Fig. 2B, C). Notably, to exclude the possibility that α -SMA⁺ and PDGFR β ⁺ cell populations were vascular smooth muscle cells (VSMCs), colocalization analysis of α -SMA and CD31 was performed.

Two other important vascular indicators, relative vessel permeability and Microvessel density (MVD), were also compared among the tumor models. HCT116 tumors

were found to exhibit the highest vessel permeability, and HT-29 tumors showed lower vessel permeability (Fig. 2D; Table 1). Furthermore, HCT116 and HT-29 tumors showed the lowest MVD and a higher MVD, respectively (Fig. 2E; Table 1). Taken together, the results indicated that in HT-29 tumors with the highest pericyte coverage, lower vessel permeability and a higher MVD were observed. Conversely, in HCT116 tumors with the lowest pericyte coverage, the highest vessel permeability and lowest MVD were observed.

Monitoring CRC models with high and low pericyte coverage by mpMRI

Previous studies have demonstrated the value of mpMRI in evaluating hemodynamics, tumor cell characteristics, and pH changes [44, 49, 54]. To investigate the feasibility of distinguishing differences in tumors with the highest and lowest pericyte coverage by mpMRI and DCE-, DWI-, and APT CEST-MRI at 9.4T was utilized to monitor the entire tumor region of the HT-29 and HCT116 models. Representative multiparametric maps of HT-29 and HCT116 CRC models are shown in Fig. 3A. In HT-29 tumors with the highest pericyte coverage, lower K^{trans} , V_e and K_{ep} values corresponded to lower relative vessel permeability, and a higher AUC value corresponded to a higher MVD (Fig. 3B). In HCT116 tumors with the lowest pericyte coverage, higher K^{trans} , V_e and K_{ep} values corresponded to higher relative vessel permeability, and a lower AUC value corresponded to a lower MVD. Additionally, significant differences were shown in ADC values and MTR_{asym} values that were calculated from the z-spectrum at $B_1 = 1.0 \mu\text{T}$ and $2.0 \mu\text{T}$ between HT-29 and HCT116 models, and the results of these differences were further investigated (Fig. 3B, C). Collectively, these results indicated that DCE- parameters on 9.4T MRI exhibited significant differences among the CRC models and were consistent with vascular characteristics.

Antitumor effect of imatinib in CRC with high pericyte coverage

To explore the antitumor effect of imatinib in CRC with excessive pericyte coverage, the effect of imatinib on HT-29 tumors with the highest pericyte coverage was evaluated by measuring the changes in tumor volume using T2-weighted imaging (T2WI), and the tumor necrosis volume was assessed through DCE imaging. Tumor volumes and necrosis volumes at each time point during imatinib treatment are shown in Fig. 4A. As shown in Tables 2 and 3, the tumor volumes of the imatinib group on Day 0, Day 4, Day 7, and Day 10 were 182.91 ± 22.29 , 229.75 ± 24.91 , 328.29 ± 15.56 , and $340.37 \pm 19.67 \text{ mm}^3$, respectively, while the tumor volumes of the control group were 186.83 ± 16.50 , 293.46 ± 22.78 , 451.09 ± 42.51 , and $578.63 \pm 47.87 \text{ mm}^3$.

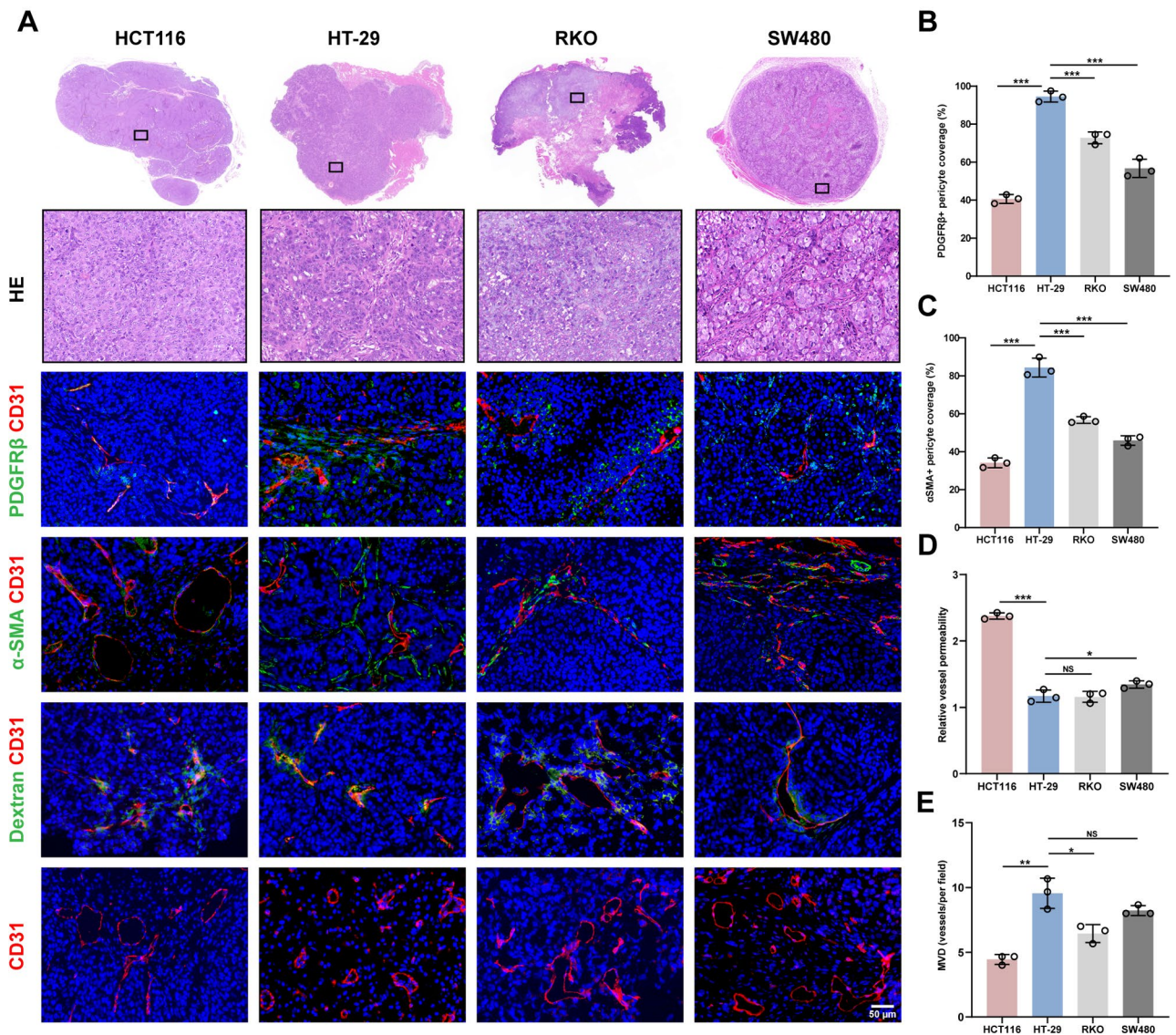


Fig. 2 Vascular characteristics in the four CRC models. **(A)** Representative images of H&E staining at high magnification and CD31/PDGFRβ, CD31/α-SMA, CD31/dextran and CD31 staining in the four CRC models. **(B)-(E)** Quantification of PDGFRβ⁺ pericyte coverage, α-SMA⁺ pericyte coverage, relative vessel permeability and the MVD in the four CRC models. The data are shown as the mean ± standard deviation. **P* < 0.05, ***P* < 0.01, ****P* < 0.001; NS, nonsignificant

Table 1 Comparison of quantitative indicators of vascular characterization in four CRC models

	HCT116	HT-29	RKO	SW480	HCT116 vs. RKO	P	
						HCT116 vs. SW480	RKO vs. SW480
PDGFRβ ⁺ pericyte coverage (%)	40.59 ± 2.30	94.51 ± 2.83	72.80 ± 3.10	56.74 ± 4.81	<0.001	<0.001	<0.001
α-SMA ⁺ pericyte coverage (%)	34.19 ± 2.56	84.34 ± 4.92	56.70 ± 1.76	45.89 ± 2.47	<0.001	0.002	0.003
Relative vessel permeability	2.38 ± 0.05	1.17 ± 0.09	1.16 ± 0.08	1.34 ± 0.05	<0.001	<0.001	0.013
MVD (vessels/per field)	4.44 ± 0.39	9.56 ± 1.17	6.44 ± 0.69	8.22 ± 0.39	0.010	<0.001	0.018

The data is presented as mean ± standard deviation. ANOVA and LSD post hoc tests were used to assess the differences in quantitative indicators among CRC models. A significance threshold of *P* < 0.05 was used for statistical significance

Starting from Day 4, the imatinib group exhibited a trend of slower growth and smaller tumor volume than the control group (Fig. 4B). Additionally, the imatinib group exhibited a smaller tumor volume change over 10 days

than the control group (Fig. 4C). Furthermore, the necrosis volumes of the imatinib group on Day 0, Day 4, Day 7, and Day 10 were 3.49 ± 0.45 , 58.10 ± 10.83 , 73.07 ± 9.61 , and 89.72 ± 10.34 mm³, while the necrosis volumes of the

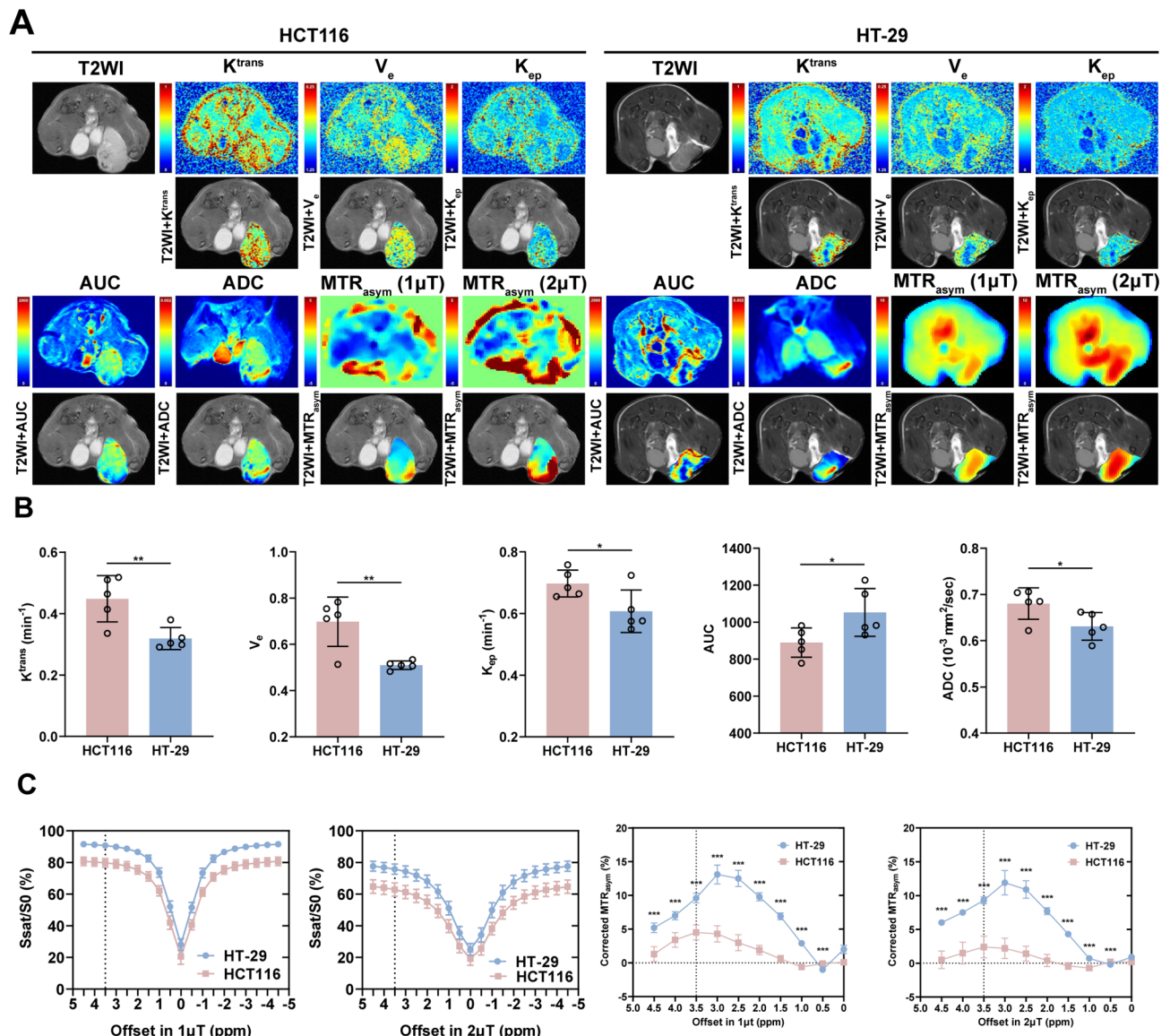


Fig. 3 9.4T mpMRI maps of CRC models with high and low pericyte coverage. **(A)** Representative T2WI images and maps of DCE-derived K^{trans} , V_e , and K_{ep} and AUC, DWI-derived ADC, and APT-CEST-derived MTR_{asym} ($1 \mu\text{T}$ and $2 \mu\text{T}$) at 3.5 ppm, of HT-29 and HCT116 tumors. **(B)** Quantification of multiple parameters, including the K^{trans} , V_e , K_{ep} , AUC, and ADC values, of HT-29 and HCT116 tumors. **(C)** Corrected-z-spectrum and MTR_{asym} values at $1 \mu\text{T}$ and $2 \mu\text{T}$ of HT-29 and HCT116 tumors. The data are shown as the mean \pm standard deviation. * $P < 0.05$, ** $P < 0.01$ and *** $P < 0.001$

control group were 3.44 ± 0.73 , 4.66 ± 0.65 , 8.15 ± 1.63 , and $17.20 \pm 2.56 \text{ mm}^3$ (Tables 2 and 3). From Day 4, the imatinib group displayed a faster tumor necrosis and larger necrosis volume than the control group (Fig. 4D). In addition, the imatinib group exhibited a higher proportion of necrosis volume compared to the control group on Day 10 (Fig. 4E). During the treatment process, mice showed no obvious abnormal reactions, and none of the mice died; however, none of the mice showed a complete tumor response. Together, the findings showed that imatinib has significant antitumor effects on CRC with high pericyte coverage but also suggested that it might not be suitable for monotherapy.

Imatinib alters vascular characteristics

To identify a proper imatinib regimen, the pattern of the pericyte coverage decrease induced by imatinib over time must be assessed. To elucidate the trends in pericyte coverage and important vascular characteristics caused by imatinib treatment, histological assessment was performed at each time point during treatment. Representative sections used to assess PDGFR β^+ pericyte coverage, $\alpha\text{-SMA}^+$ pericyte coverage, MVD, and relative vessel permeability during treatment are shown in Fig. 5A. In the imatinib group, intratumor PDGFR β^+ pericyte coverage and $\alpha\text{-SMA}^+$ pericyte coverage both showed a decreasing trend (Fig. 5B; Tables 2 and 3). PDGFR β^+

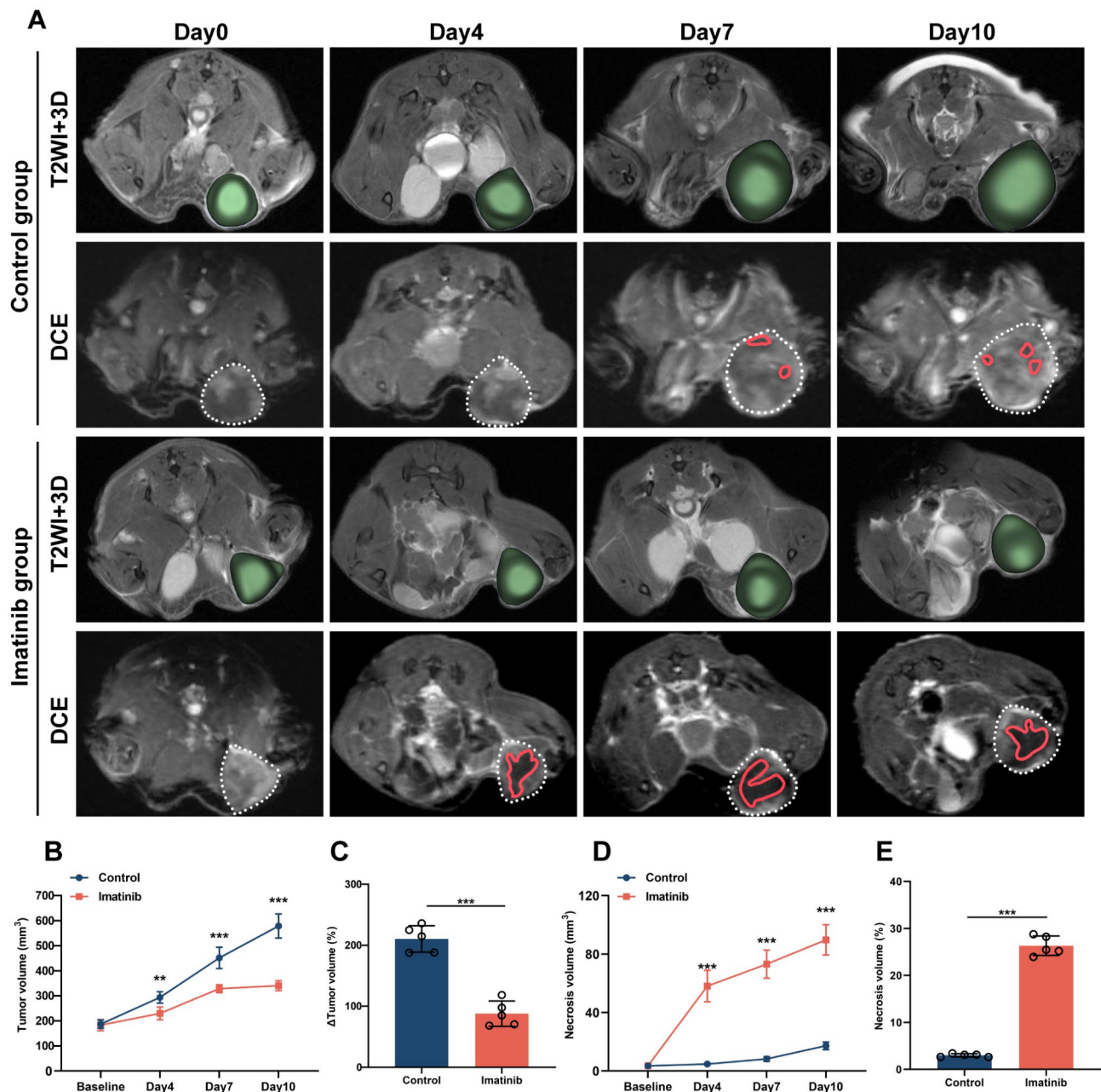


Fig. 4 Antitumor effect to imatinib treatment in CRC with high pericyte coverage. (A) Representative T2WI and DCE images used for HT-29 tumor volume and necrosis volume measurement during imatinib treatment. (B) Curves of tumor volumes of the imatinib group and control group measured at different timepoints. (C) Quantification of tumor volume changes in the two groups. (D) Curves of necrosis volumes of the imatinib group and control group measured at different timepoints. (E) Proportion of necrosis volume in the two groups. The data are shown as the mean \pm standard deviation. * $P < 0.05$, ** $P < 0.01$ and *** $P < 0.001$

pericyte coverage gradually declined from Day 0 to Day 7, reaching a plateau after Day 7 ($F = 186.22$, $P < 0.001$). Similarly, α -SMA⁺ pericyte coverage declined gradually in the first 4 days, subsequently showed a slower decrease and reached a plateau after Day 7 ($F = 119.112$, $P < 0.001$). Additionally, relative vessel permeability gradually increased from Day 0 to Day 7, reaching a plateau after Day 7 ($F = 12.867$, $P = 0.002$, Fig. 5B; Tables 2 and 3).

Subsequently, the MVD showed a gradual decline from day 0 to day 4, a significant decline from Day 4 to Day 7, and then a slower gradual decline after Day 7 ($F = 35.952$, $P < 0.001$, Fig. 5B; Tables 2 and 3). There were no significant trends observed for any of the indicators among the control group ($P > 0.05$). Starting from Day 4, significant differences were observed in PDGFR- β ⁺ pericyte coverage, α -SMA⁺ pericyte coverage, MVD and relative vessel

Table 2 Quantitative variations of tumor volume, histological and imaging results in control group

Control group	Day0	Day4	Day7	Day10	F	P
Tumor volume (mm ³)	186.83 ± 16.50	293.46 ± 22.78	451.09 ± 42.51	578.63 ± 47.87	121.726	0.001
Necrosis volume (mm ³)	3.44 ± 0.73	4.66 ± 0.65	8.15 ± 1.63	17.20 ± 2.56	81.249	0.001
PDGFRβ ⁺ pericyte coverage (%)	94.22 ± 5.23	84.34 ± 3.10	90.36 ± 2.92	87.68 ± 5.68	2.678	0.118
α-SMA ⁺ pericyte coverage (%)	84.76 ± 3.58	87.57 ± 4.67	86.16 ± 2.45	91.88 ± 2.45	2.459	0.137
Relative vessel permeability	1.16 ± 0.21	1.25 ± 0.08	1.14 ± 0.14	1.27 ± 0.10	0.598	0.634
MVD (vessels/per field)	9.33 ± 0.67	9.78 ± 0.39	9.11 ± 0.39	9.44 ± 0.70	0.758	0.548
Ki-67 (%)	28.28 ± 1.08	30.73 ± 1.39	28.01 ± 1.26	27.55 ± 1.91	2.981	0.096
TUNEL (%)	7.59 ± 1.37	19.27 ± 1.91	21.11 ± 2.30	30.54 ± 2.53	61.082	0.001
HIF-1α (%)	38.12 ± 0.81	39.69 ± 1.80	39.94 ± 1.17	40.00 ± 1.01	1.572	0.270
Mcl-1 (%)	36.05 ± 0.37	38.50 ± 1.24	36.64 ± 2.85	38.00 ± 1.47	1.302	0.339
K ^{trans} (min ⁻¹)	0.31 ± 0.02	0.34 ± 0.03	0.33 ± 0.04	0.32 ± 0.04	0.569	0.643
V _e	0.52 ± 0.01	0.56 ± 0.03	0.54 ± 0.04	0.53 ± 0.01	1.317	0.303
K _{ep} (min ⁻¹)	0.61 ± 0.02	0.61 ± 0.03	0.60 ± 0.08	0.60 ± 0.07	0.033	0.992
AUC	1028.49 ± 73.39	955.03 ± 143.60	982.23 ± 105.65	955.17 ± 68.81	0.572	0.641
ADC (×10 ⁻³ mm ² /sec)	0.62 ± 0.02	0.62 ± 0.03	0.64 ± 0.02	0.66 ± 0.03	1.800	0.188
MTR _{asym} (1 μT, %)	8.97 ± 0.27	8.14 ± 1.42	8.37 ± 0.65	7.41 ± 0.85	2.550	0.092
MTR _{asym} (2 μT, %)	9.05 ± 0.30	7.94 ± 1.23	8.22 ± 0.75	7.73 ± 1.35	1.702	0.207

The data is presented as mean ± standard deviation. ANOVA were used to assess the differences in parameters among different time points within each group. A significance threshold of $P < 0.05$ was used for statistical significance

Table 3 Quantitative variations of tumor volume, histological and imaging results in imatinib group

Imatinib group	Day0	Day4	Day7	Day10	F	P
Tumor volume (mm ³)	182.91 ± 22.29	229.75 ± 24.91	328.29 ± 15.56	340.37 ± 19.67	67.012	0.001
Necrosis volume (mm ³)	3.49 ± 0.45	58.10 ± 10.83	73.07 ± 9.61	89.72 ± 10.34	88.168	0.001
PDGFRβ ⁺ pericyte coverage (%)	94.17 ± 4.77	75.10 ± 3.45	41.57 ± 2.14	40.05 ± 2.46	186.22	0.001
α-SMA ⁺ pericyte coverage (%)	83.55 ± 5.31	50.46 ± 3.27	34.16 ± 3.41	30.96 ± 2.84	119.112	0.001
Relative vessel permeability	1.16 ± 0.23	1.56 ± 0.09	1.86 ± 0.13	1.90 ± 0.17	12.867	0.002
MVD (vessels/per field)	9.33 ± 0.67	8.22 ± 0.39	5.67 ± 0.58	5.56 ± 0.51	35.952	0.001
Ki-67 (%)	28.16 ± 1.09	19.13 ± 1.60	14.61 ± 1.23	8.74 ± 1.43	109.248	0.001
TUNEL (%)	7.59 ± 1.14	23.99 ± 1.83	44.64 ± 2.05	56.99 ± 1.86	460.606	0.001
HIF-1α (%)	38.03 ± 1.02	32.71 ± 1.02	35.68 ± 1.88	44.72 ± 1.71	37.043	0.001
Mcl-1 (%)	36.10 ± 1.54	32.19 ± 1.36	15.73 ± 1.29	15.81 ± 2.17	130.236	0.001
K ^{trans} (min ⁻¹)	0.31 ± 0.04	0.48 ± 0.03	0.55 ± 0.04	0.60 ± 0.02	70.465	0.001
V _e	0.51 ± 0.02	0.63 ± 0.04	0.66 ± 0.03	0.72 ± 0.06	24.004	0.001
K _{ep} (min ⁻¹)	0.61 ± 0.08	0.77 ± 0.06	0.90 ± 0.07	0.88 ± 0.06	18.626	0.001
AUC	1027.37 ± 94.51	688.80 ± 82.65	581.11 ± 60.46	555.44 ± 42.59	44.470	0.001
ADC (×10 ⁻³ mm ² /sec)	0.63 ± 0.04	0.68 ± 0.02	0.75 ± 0.03	0.83 ± 0.02	45.103	0.001
MTR _{asym} (1 μT, %)	9.03 ± 0.38	9.73 ± 0.55	6.91 ± 1.10	7.31 ± 1.07	12.701	0.001
MTR _{asym} (2 μT, %)	9.04 ± 0.52	9.64 ± 0.20	7.88 ± 1.35	8.02 ± 0.86	4.904	0.013

The data is presented as mean ± standard deviation. ANOVA were used to assess the differences in parameters among different time points within each group. A significance threshold of $P < 0.05$ was used for statistical significance

permeability between the two groups. Taken together, these data demonstrated that the imatinib-induced decrease in pericyte coverage reached a plateau on Day 7 and was accompanied by increased vessel permeability and decreased MVD in CRC with high pericyte coverage.

Molecular and histological profiling of treatment-induced TME alterations

A previous study demonstrated that imatinib down-regulates the expression of Bcl-w, a component of the Bcl-2/bax pathway, in tumor ECs [42]. However, the

relationship between the Bcl-2/bax pathway and imatinib-mediated modulation of pericyte coverage remains unknown. To explore whether imatinib modulated the gene expression of Bcl-2/bax pathway components, the expression of key genes in the Bcl-2/bax pathway and the related gene *AKT1* was compared between the imatinib and control groups on Day 10. In the imatinib group, the mRNA expression of antiapoptotic genes, such as *MCL-1*, *BCL-2*, *BCL-W*, *BCL-XL*, and *AKT-1*, was significantly downregulated, while that of proapoptotic genes, such as *BAX*, *BAK*, *CASP3*, and *CASP8*, was significantly

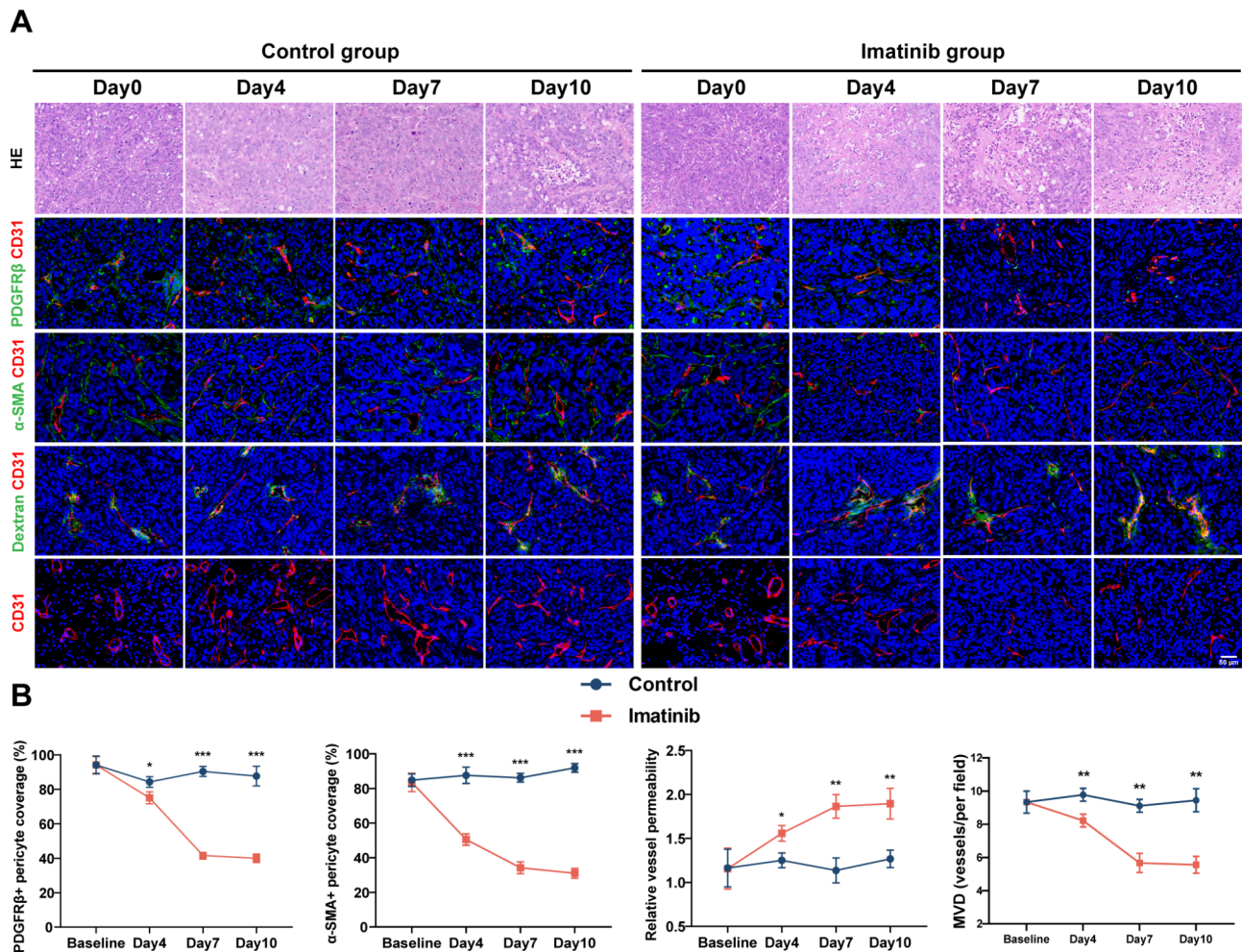


Fig. 5 Histological assessment of vascular characteristics at different time points during imatinib treatment. **(A)** Representative images of H&E, CD31/PDGFR β , CD31/ α -SMA, CD31/dextran and CD31 staining during treatment. **(B)** Longitudinal assessments of vascular characteristics, including PDGFR β ⁺ pericyte coverage, α -SMA⁺ pericyte coverage, relative vessel permeability and the MVD, in the imatinib group and control group. The data are shown as the mean \pm standard deviation. * $P < 0.05$, ** $P < 0.01$, *** $P < 0.001$; NS, nonsignificant

upregulated (Fig. 6A). *MCL-1* is a multidrug resistance gene, and *Mcl-1* overexpression indicates inhibition of tumor apoptosis and resistance to multiple antitumor therapies [39–41]. More importantly, an inappropriate decrease in pericyte coverage leads to increased hypoxia-associated metastasis and decreased survival, highlighting that elucidating the impact of imatinib treatments on TME hypoxia is crucial for identifying a proper imatinib regimen. To elucidate the trends in tumor apoptosis and TME hypoxia induced by imatinib, the expression of the antiapoptotic protein *Mcl-1*, proliferation marker *Ki-67*, and TME hypoxia marker *HIF-1 α* and apoptosis, which was assessed by TUNEL staining, during treatment were evaluated by IF staining; representative sections are shown in Fig. 6B. In the imatinib group, a significant decrease in *Ki-67* expression was observed in tumors, indicating inhibition of tumor proliferation ($F = 109.248$, $P < 0.001$, Fig. 6C; Tables 2 and 3). Similarly, a significant

increase in the intensity of TUNEL staining, which was used to assess apoptosis, and a significant decrease in the expression of the anti-apoptotic protein *Mcl-1* indicated increased tumor apoptosis ($F = 460.606$, $P < 0.001$ for TUNEL and $F = 130.236$, $P < 0.001$ for *Mcl-1*, Fig. 6C; Tables 2 and 3). Notably, *HIF-1 α* expression showed a slow decline from Day 0 to Day 4, followed by a gradual increase after Day 4, suggesting alleviation followed by aggravation of TME hypoxia ($F = 37.043$, $P < 0.001$, Fig. 6C; Tables 2 and 3). Among the control group, no significant trends were observed in *Ki-67*, *HIF-1 α* , or *Mcl-1* expression, but there was a mild upward trend in the TUNEL staining intensity. Starting from Day 4, *Ki-67*, TUNEL, *HIF-1 α* , and *Mcl-1* expression was significantly different between the two groups. According to hematoxylin and eosin (HE) staining, there was a large area of tumor necrosis from Day 4 in the imatinib group, while only a small area of necrosis was observed on Day 10 in

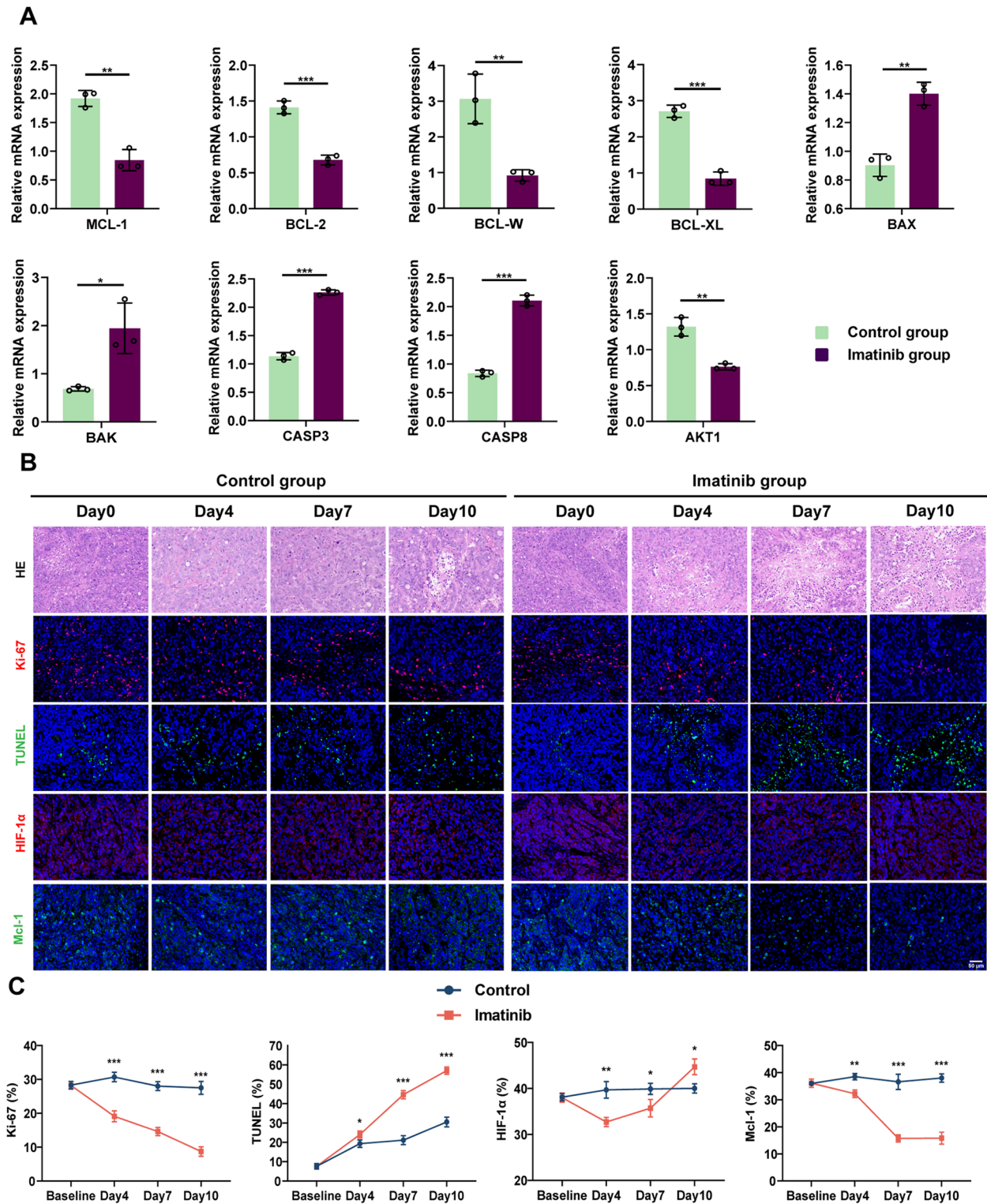


Fig. 6 qPCR analysis of the gene expression of Bcl-2/Bax pathway components and histological assessment of TME indicators during imatinib treatment. **(A)** qPCR analysis of the gene expression of Bcl-2/Bax pathway components in the imatinib group and control group on Day 10. **(B)** Representative images of H&E, Ki-67, TUNEL, HIF-1α and Mcl-1 staining during treatment. **(C)** Longitudinal assessment of TME indicators, including Ki-67 expression, the TUNEL staining intensity, HIF-1α expression and Mcl-1 expression, in the two groups. The data are shown as the mean ± standard deviation. **P* < 0.05, ***P* < 0.01, ****P* < 0.001; NS, nonsignificant

the control group. Together, these data indicated that imatinib induces tumor apoptosis through the Bcl-2/bax pathway and that 4 days of imatinib treatment alleviates hypoxia in CRC with high pericyte coverage.

Alterations of mpMRI parameters during imatinib treatment

mpMRI has the potential to overcome the limitations of histological for longitudinal monitoring of pericyte coverage, and is thus a potential technique for evaluating of the effects of imatinib treatment. To prove this hypothesis, DCE-, DWI-, and APT CEST-MRI were conducted to monitor the effects of 10-day imatinib treatment. Representative multiparametric maps obtained during imatinib treatment are shown in Fig. 7A. The influence of imatinib treatment on tumor hemodynamics was reflected by changes in DCE-MRI parameters, including K^{trans} , V_e , K_{ep} , and the AUC. In the imatinib group, increasing trends in the K^{trans} , V_e , and K_{ep} values were observed in the tumor region, suggesting increased vessel permeability (Fig. 7B; Tables 2 and 3). First, the K^{trans} value significantly increased from Day 0 to Day 4 of treatment, followed by a gradual increase ($F=70.465$, $P<0.001$). Second, the V_e value increased significantly from Day 0 to Day 4, followed by a gradual increase, and increased significantly again after Day 7 ($F=24.004$, $P<0.001$). Third, the K_{ep} value exhibited a significant increase from Day 0 to Day 7, reaching a plateau after Day 7 ($F=18.626$, $P<0.001$). Moreover, a decline in the AUC in the tumor region was noticed in the imatinib group, indicating a reduction in vascular volume (Fig. 7B; Tables 2 and 3). The AUC significantly decreased from Day 0 to Day 4, followed by a gradual decline, and reached a plateau after Day 7 in the imatinib group ($F=44.470$, $P<0.001$). The control group showed no significant trend in any of the parameters ($P>0.05$). Starting from Day 4, a significant difference was observed in the K^{trans} , V_e , K_{ep} , values and AUC between the two groups. Together, the results indicated that the DCE-derived K^{trans} , V_e and K_{ep} values were sensitive indicators of increased vessel permeability induced by a decrease in pericyte coverage and that the AUC reflected the reduced accumulation of the contrast agent.

To evaluate the feasibility of using DWI- and APT CEST-MRI to quantify TME alterations, DWI-derived ADC and APT CEST-derived MTR_{asym} values were longitudinally monitored during imatinib treatment. In the imatinib group, there was a moderate increase in the intratumor ADC value ($F=45.103$, $P<0.001$), indicating increased diffusion of water molecules and increased tumor necrosis (Fig. 7B; Tables 2 and 3). Moreover, the MTR_{asym} value increased initially, followed by a subsequent decrease, indicating a pH change in the TME (Fig. 7B; Tables 2 and 3). At $B1=1 \mu\text{T}$ and $2 \mu\text{T}$, the

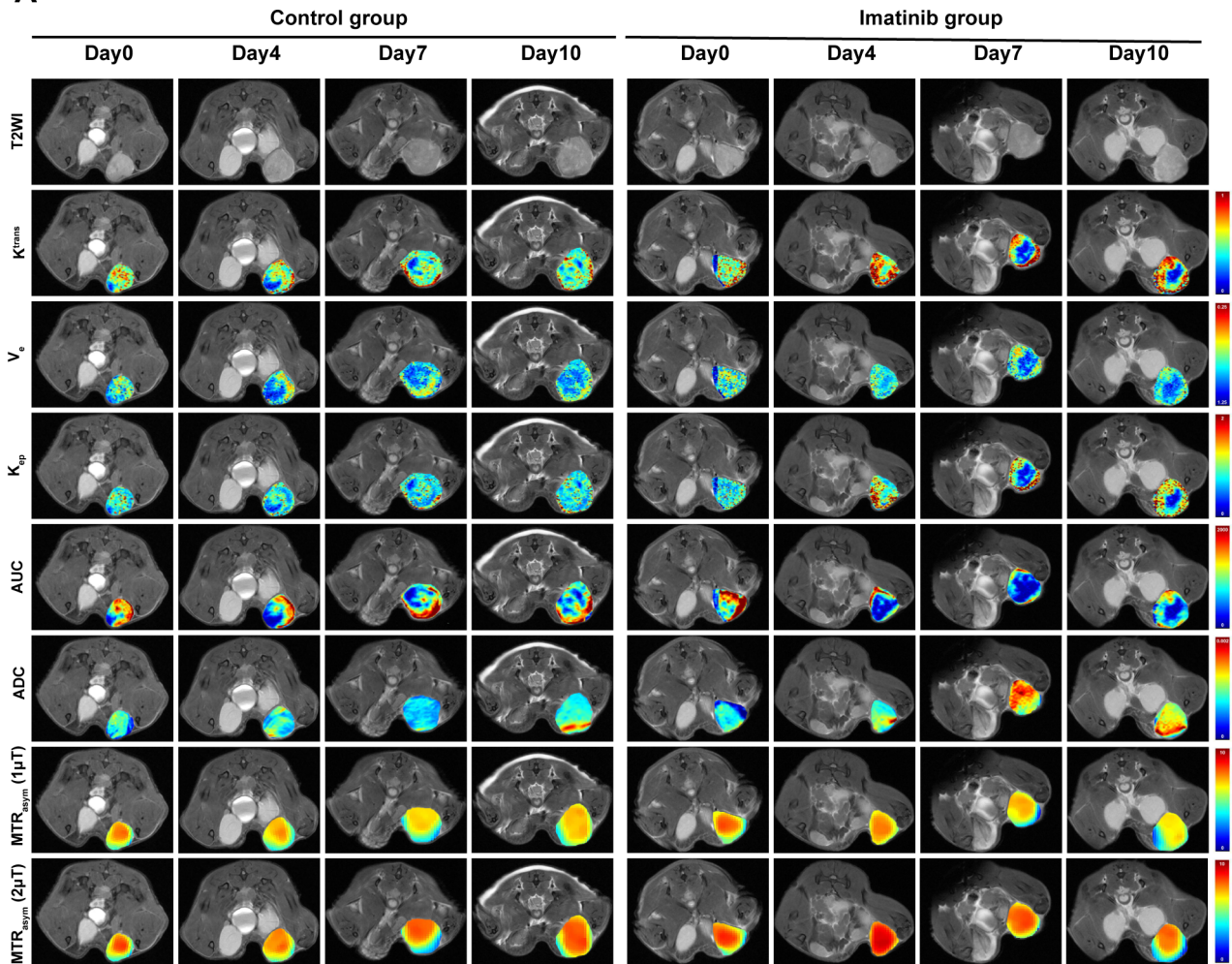
MTR_{asym} value showed a gradual increase from Day 0 to Day 4, followed by a gradual decline after Day 4 ($F=12.701$, $P<0.001$ for $B1=1 \mu\text{T}$ and $F=4.904$, $P=0.013$ for $B1=2 \mu\text{T}$). The trend in the MTR_{asym} value was more pronounced at $B1=1 \mu\text{T}$ than at $B1=2 \mu\text{T}$. There were no significant trends observed for any of the parameters among the control group ($P>0.05$). From Day 4, there were significant differences observed in the ADC value between the two groups. Significant differences in only the MTR_{asym} value were observed on Day 4 at $B1=1 \mu\text{T}$ and $2 \mu\text{T}$ and on Day 7 at $B1=1.0 \mu\text{T}$. Collectively, the findings indicated that the DWI-derived ADC value was sensitive reflecting increased diffusion of water molecules due to imatinib-induced tumor necrosis, and the APT CEST-derived MTR_{asym} ($1 \mu\text{T}$) value for reflecting pH level was experiencing a 4-day increase followed by a subsequent decline.

Correlation analysis of the changes induced by imatinib treatment

To investigate the correlation between pericyte coverage and TME indicators after imatinib treatment, correlation analysis among the histological data was conducted, and the results are shown in Fig. 8A. Among vascular features, $\text{PDGFR}\beta^+$ pericyte coverage showed the strongest positive correlation with $\alpha\text{-SMA}^+$ pericyte coverage ($r=0.90$, $P<0.01$). Moreover, relative vessel permeability was negatively correlated with $\text{PDGFR}\beta^+$ pericyte coverage ($r=-0.71$, $P<0.05$). Furthermore, the MVD exhibited a positive correlation with $\text{PDGFR}\beta^+$ pericyte coverage ($r=0.80$, $P<0.05$). Regarding the correlation between vascular and TME indicators, Mcl-1 expression was positively correlated with $\text{PDGFR}\beta^+$ pericyte coverage ($r=0.90$, $P<0.01$) and $\alpha\text{-SMA}^+$ pericyte coverage ($r=0.86$, $P<0.01$). Additionally, HIF-1 α expression was negatively correlated with $\text{PDGFR}\beta^+$ pericyte coverage ($r=-0.76$, $P<0.05$). $\text{PDGFR}\beta^+$ pericyte coverage displayed a significant correlation with Ki-67 expression and the TUNEL staining intensity (Ki-67: $r=0.72$ ($P<0.05$) and TUNEL: $r=-0.76$ ($P<0.05$)), indicating that imatinib had an antitumor effect. Taken together, the results showed that $\text{PDGFR}\beta^+$ pericyte coverage is not only correlated with vessel-related $\alpha\text{-SMA}^+$ pericyte coverage, vessel permeability and the MVD but also correlated with Ki-67, TUNEL, HIF-1 α and Mcl-1 expression in the TME during imatinib treatment.

To identify MRI parameters for histological indicators that maybe useful for monitoring the treatment effect of imatinib, correlation analysis between MRI and histological data was conducted, and the results are shown in Fig. 8B and C. In terms of vascular characteristics, the permeability-related parameter V_e showed a very strong correlation with $\text{PDGFR}\beta^+$ pericyte coverage ($r=-0.89$, $P<0.01$). Moreover, K^{trans} exhibited the strongest

A



B

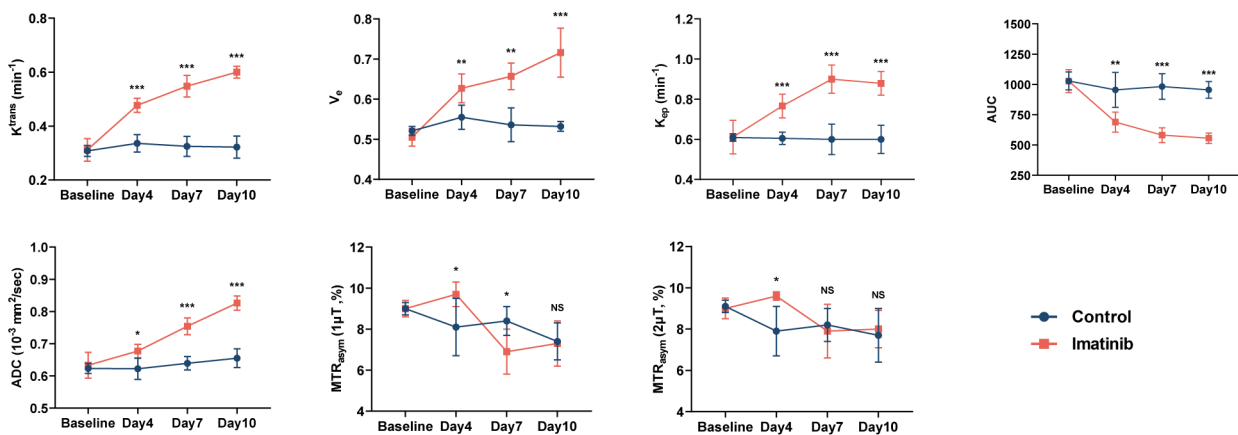


Fig. 7 mpMRI monitoring of the CRC model with high pericyte coverage during imatinib treatment. **(A)** Representative T2WI images and maps of DCE-derived K^{trans} , V_e , and K_{ep} and AUC, DWI-derived ADC, and APT-CEST-derived MTR_{asym} (1 μT and 2 μT) at 3.5 ppm during treatment. **(B)** Longitudinal assessment of multiple parameters, including the K^{trans} , V_e , and K_{ep} , AUC, ADC, and MTR_{asym} (1 μT and 2 μT) values, in the imatinib group and control group. The data are shown as the mean \pm standard deviation. * $P < 0.05$, ** $P < 0.01$, *** $P < 0.001$; NS, nonsignificant

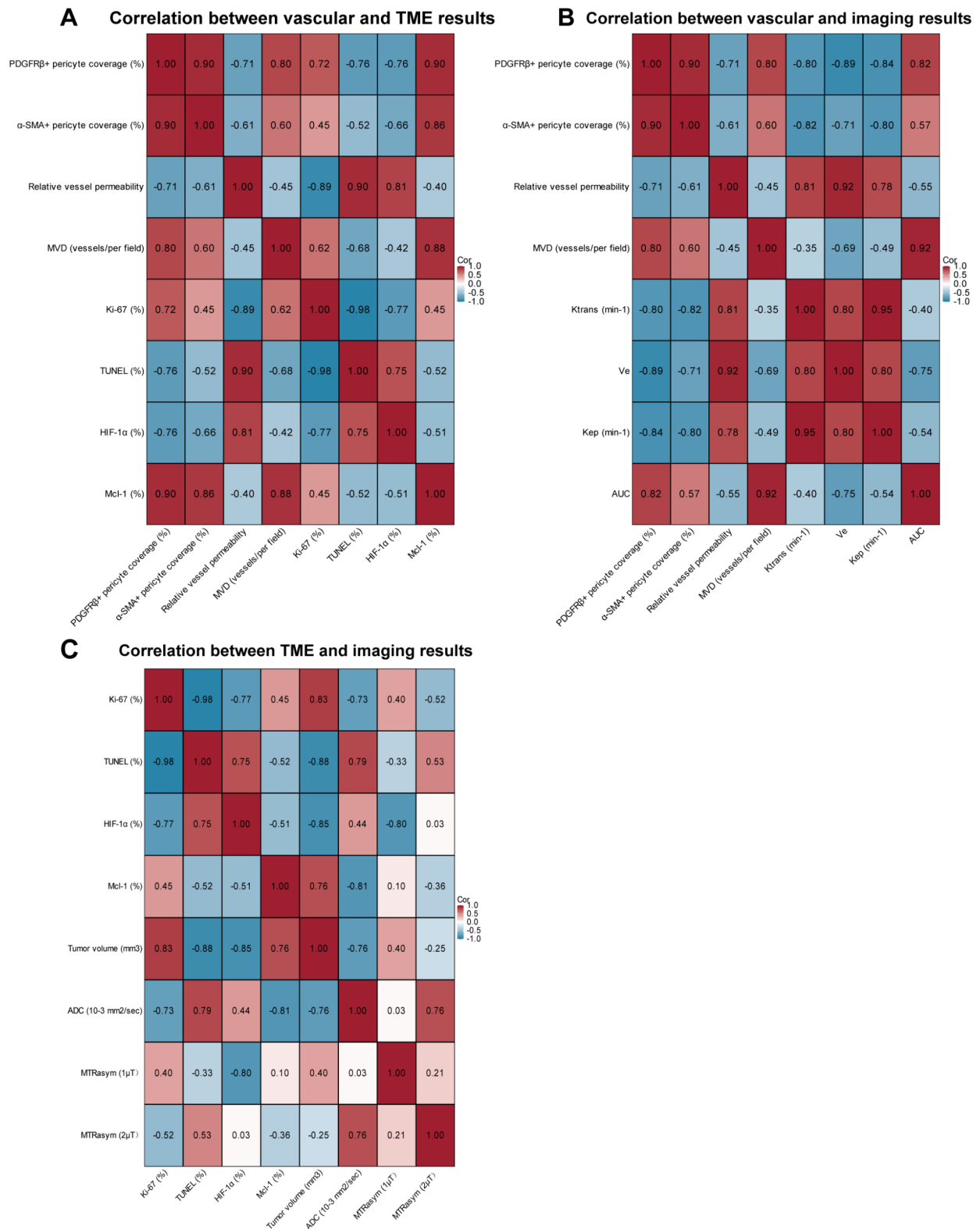


Fig. 8 Correlation analysis among the histological results and between the imaging and histological results

correlation with α -SMA⁺ pericyte coverage ($r = -0.82$, $P < 0.05$). The parameter that was the most strongly correlated with V_e was relative vessel permeability ($r = 0.92$, $P < 0.01$). The perfusion-related parameter AUC exhibited a positive correlation with the MVD ($r = 0.92$, $P < 0.01$). In terms of TME indicators, the ADC value strongly correlated with Ki-67 and Mcl-1 expression and the TUNEL staining intensity (Ki-67: $r = -0.73$ ($P < 0.05$), TUNEL: $r = 0.79$ ($P < 0.05$), and Mcl-1: $r = -0.81$ ($P < 0.05$)). Tumor volume was most strongly correlated with TUNEL ($r = -0.88$, $P < 0.01$). Moreover, the MTR_{asym} (1 μ T) value showed a negative correlation with HIF-1 α expression (MTR_{asym} (1 μ T): $r = -0.80$ ($P < 0.05$)). Collectively, the findings showed that MRI and histological data were well correlated, indicating that V_e and K^{trans} are useful for evaluating pericyte coverage, V_e for vessel permeability, the AUC for MVD, the ADC for tumor apoptosis and the MTR_{asym} value at 1 μ T for HIF-1 α expression during imatinib treatment.

Discussion

Antiangiogenic therapies turn off angiogenic switches to inhibit tumor vessel growth and starve tumors and are recommended for the treatment of advanced CRC by the NCCN guidelines [2–4]. Vascular pericytes play an important role in the TME, but the value of targeting pericytes by common antiangiogenic therapies has been overlooked [7, 67]. The unclear efficacy of imatinib in effectively combating tumors and angiogenesis in CRC with high pericyte coverage is attributed to the complex interactions between pericytes and the TME [68, 69]. There is an urgent need to develop an effective imatinib strategy to treat tumors and boost antitumor drug efficacy. It has been confirmed that pericyte coverage and TME hypoxia are significant influencing factors of treatment efficacy [17, 36]. Thus, the rational strategy for targeting pericytes is based on clarifying the correlation of pericyte coverage and TME indicators, and emphasizing at constructing an appropriate monitoring technique. Here, we provide an effective imatinib strategy in CRC with high pericyte coverage and reported a noninvasive approach to monitor changes in pericyte coverage and TME indicators by 9.4T mpMRI. DCE- parameters were shown to be histologic match the tumor vascular characterizations among CRC with high and low pericyte coverage. Excessive pericyte coverage was shown to increase the tumor growth rate in a previous study, and our results confirmed the significant antitumor effect of imatinib in the presence of high pericyte coverage [35]. Consistent with a previous study, decreased pericyte coverage, increased vascular permeability, inhibited vascular growth and increased tumor apoptosis were observed during treatment [17]. One of the findings was that an increase in tumor apoptosis might be related to

imatinib-induced upregulation of proapoptotic genes and downregulation of antiapoptotic genes in the Bcl-2/Bax pathway. Another finding was that the decrease in pericyte coverage finally reached a plateau. A 4-day treatment regimen significantly reduced pericyte coverage and HIF-1 α expression, while the decrease in pericyte coverage became less marked and HIF-1 α expression was restored with prolonged treatment. The strongest correlation between MRI parameters and histological results indicated that V_e and K^{trans} were good indicators of pericyte coverage, V_e of vessel permeability, the AUC of the MVD, the ADC of tumor apoptosis, and the MTR_{asym} value at 1 μ T of HIF-1 α expression and hypoxia.

Various cell components, including tumor cells, inflammatory cells, fibroblasts, progenitor cells, vascular ECs and pericytes, are known to exist in the TME. Although pericytes constitute a fundamental element of the TME, the beneficial effects of imatinib regimen in treating tumors remains unknown [7]. An increasing number of studies have indicated that an overabundance of pericytes promotes tumor progression and decreases anti-tumor drug efficacy [21, 28, 32]. In contrast, insufficient pericyte coverage indicates an increased capacity for tumor metastasis, highlighting the necessity for selective decreases in pericyte coverage [17]. Hence, selectively decreasing pericyte coverage when it is excessive might be a reasonable approach for treating tumors. To confirm this assumption in a CRC model with high pericyte coverage, the degree of pericyte coverage was first determined by IF staining in different CRC models. Due to the lack of specific markers, the identification of pericytes relies on a combination of morphological criteria and staining with multiple markers, including PDGFR β , a marker of immature pericytes, and α -SMA, a marker of mature pericytes [9, 70]. Among the four CRC models, the highest pericyte coverage was observed in HT-29 tumors and was accompanied by a higher MVD; the lowest pericyte coverage and MVD was observed in HCT116 tumors (Fig. 2B, C, E; Table 1). In contrast, lower vessel permeability was seen in HT-29 tumors, which had the highest pericyte coverage, while the highest vessel permeability was observed in HCT116 tumors, which had the lowest pericyte coverage (Fig. 2B-D; Table 1). Similarly, pericyte coverage correlates positively with the MVD and poor prognosis in renal cancer, while impacting vessel permeability in the gliomas study [71, 72]. Subsequently, the HT-29 model, which had the highest pericyte coverage, and the HCT116 model, which had the lowest pericyte coverage, were selected and used for DCE-, DWI-, and APT CEST-MRI. The differences in MRI parameters showed consistency with differences in vascular characteristics, as lower K^{trans} , V_e and K_{ep} values matched with lower vessel permeability were observed in the model with higher pericyte coverage, and higher

K^{trans} , V_e and K_{ep} values corresponded to higher vessel permeability in the model with lower pericyte coverage (Fig. 3B). Furthermore, the AUC also exhibited a match with the MVD. Moreover, we selected the CRC model with high pericyte coverage for research on the effect of our imatinib treatment strategy and further explored the value of MRI parameters in monitoring the treatment effect.

Next, the antitumor effect of imatinib in CRC with high pericyte coverage was explored. Based on T2WI-based tumor volume and DCE-based necrosis volume measurements, significant tumor growth inhibition and increased tumor necrosis were observed in the imatinib group (Fig. 4A). During imatinib treatment, in addition to showing a slower growth trend and smaller tumor volume change, tumors also exhibited a faster tumor necrosis trend and higher necrosis volume proportion (Fig. 4B-E; Tables 2 and 3). According to the H&E staining, a large area of tumor necrosis was observed in the imatinib group from Day 4, while only a small area of tumor necrosis was seen in the control group on Day 10 (Fig. 5A). We confirmed the significant antitumor effect of imatinib in CRC with high pericyte coverage at the macroscopic and microscopic levels, expanding on previous studies [17, 73]. Importantly, mice exhibited good tolerance for imatinib, showing no obvious abnormal reactions, but imatinib did not result in complete tumor remission and therefore might not be suitable for monotherapy in CRC.

To optimize the imatinib regimen in CRC with high pericyte coverage, a rational treatment approach and a noninvasive evaluation approach are needed. First, an effective treatment strategy was proposed considering the ability of imatinib to regulate pericyte coverage and the TME. Second, histological analysis is invasive and cannot be performed continuously, thus, it is not suitable for longitudinal monitoring of the effects of imatinib. Thus, it is essential to establish a noninvasive evaluation approach and identify representative imaging biomarkers for monitoring pericyte coverage and changes in the TME in response to treatment. Based on the experimental results of this study, in CRC with high pericyte coverage, our imatinib treatment strategy resulted in a significant decrease in PDGFR β^+ and α -SMA $^+$ pericyte coverage within the first 4 days (Fig. 5B; Tables 2 and 3). From Day 4 to Day 7, a more gradual decrease in α -SMA $^+$ pericyte coverage was observed, suggesting that the effect of our imatinib treatment strategy became weaker; however, a continuous decrease in PDGFR β^+ pericyte coverage may be attributed to vascular maturation during tumor development [36]. In addition, pericytes are continuously recruited during tumor development, which is regulated by PDGF-BB, heparin-binding EGF-like growth factor (HB-EGF) and stromal derived factor-1 α (SDF-1 α)

[34, 74–76]. PDGFR β^+ and α -SMA $^+$ pericyte coverage reached a plateau on Day 7, suggesting establishment of a balance between imatinib-induced pericyte depletion and pericyte recruitment. Similar to previous research findings, an increase in vessel permeability and a decrease in the MVD were observed during imatinib treatment (Fig. 5B; Tables 2 and 3) [17]. A longitudinal evaluation system would not only allow trends in pericyte coverage and TME indicators to be observed but also allow for personalized adjustments during imatinib treatment. In previous research, Shi et al. utilized DCE-MRI to evaluate the effect of a vascular disrupting agent in pulmonary malignancy and found that the K^{trans} value can predict vascular disruption by reflecting hemodynamic changes [43]. Thus, we hypothesized that DCE-MRI can also be used to monitor hemodynamic changes during imatinib treatment. We found that K^{trans} , the contrast agent efflux transfer constant, which is commonly employed to assess vessel permeability and perfusion, increased. According to the histological results, the increase in K^{trans} suggests that imatinib led to elevated vessel permeability and contrast agent leakage, which was caused by decreased pericyte coverage (Fig. 7B; Tables 2 and 3). Additionally, an increase in the extravascular extracellular volume fraction V_e and contrast agent reflux transfer constant K_{ep} similarly indicated an increase in vessel permeability. The semiquantitative parameter AUC reflects the amount of contrast agent accumulated in the tumor region, which is related to angiogenesis [77]. The AUC significantly decreased from Day 0 to Day 4, subsequently showed a more gradual decrease, and stabilized after Day 7, confirming that imatinib had an antiangiogenic effect [32, 42]. After Day 7, both the K^{trans} and K_{ep} value showed a more gradual increase, similar to the plateau observed for pericyte coverage. Compared to the K^{trans} and K_{ep} value, the V_e value exhibited a consistent trend from Day 0 to Day 7 but increased significantly after Day 7. A previous study reported that imatinib reduces extracellular matrix (ECM) fibrosis and interstitial fluid pressure (IFP) in ECM-rich CRC [73]. As imatinib targets both pericytes and fibroblasts, the elevation of the V_e value suggests not only increased vessel permeability but also decreased IFP. Our speculation that the V_e value reflects IFP changes during imatinib treatment requires further validation. According to the correlation analysis, the V_e and K^{trans} values showed the strongest correlation with PDGFR β^+ pericyte coverage and α -SMA $^+$ pericyte coverage, while the V_e value was strongly correlated with relative vessel permeability. The semiquantitative parameter AUC strongly correlated with the MVD. These results indicate that a multiple evaluating potential of V_e and when combined, V_e and K^{trans} can act as excellent imaging indicators of pericyte coverage during imatinib treatment.

Mcl-1, a component of the Bcl-2/bax apoptosis pathway, is known to be overexpressed in malignancies [37, 78]. Mcl-1 is a multidrug resistance gene, and Mcl-1 overexpression is a significant factor contributing to the resistance of malignancies to radiotherapy, chemotherapy, and antiangiogenic therapy [38–41]. Through qPCR analysis, we confirmed downregulated mRNA expression of anti-apoptotic genes, including MCL-1, and upregulation of pro-apoptotic genes in the Bcl-2/bax pathway after imatinib treatment (Fig. 6A). A gradual increase in Mcl-1 protein expression was also demonstrated by IF staining during the treatment process (Fig. 6C; Tables 2 and 3). Additionally, the decrease in the expression of the proliferation marker Ki-67 and increase in the density of TUNEL staining, which was used to assess apoptosis, in CRC tissues confirmed imatinib's effect in inhibiting proliferation and promoting apoptosis. Lei et al. utilized DWI-MRI to monitor the free diffusion of water molecules in the tumor region, reflecting cell density and tumor necrosis [49]. In our study, DWI-MRI was applied to assess the tumor cell response, and a gradual increase in the ADC value was observed during imatinib treatment (Fig. 7B; Tables 2 and 3). This increase might be attributed to imatinib-induced tumor necrosis and liquefaction, leading to increased diffusion of water molecules. Furthermore, there were strong correlations between the ADC value and Ki-67 expression, the TUNEL staining intensity, and Mcl-1 expression, indicating that the ADC value can be used to monitor tumor proliferation and apoptosis during imatinib treatment.

Intratumoral hypoxia has a great impact on the role of pericytes in tumor progression. In a recent study, a reduction in pericyte number inhibited tumor growth and metastasis under normoxic conditions but promoted tumor progression under hypoxic conditions [36]. Another study also reported that poor pericyte coverage led to the promotion of HIF-1 α expression and hypoxia-driven metastasis [17]. Therefore, monitoring changes in TME hypoxia is crucial for developing an effective imatinib treatment strategy. HIF-1 α is a hallmark indicator of hypoxia, including in the TME [79]. Decreases in pericyte coverage and HIF-1 α expression were confirmed after 4 days of imatinib treatment, while continuous targeting of pericytes resulted in weakened regulation of pericyte coverage and re-elevation of HIF-1 α expression (Fig. 6C; Tables 2 and 3). APT CEST-MRI, which can sensitively reflect changes in pH without the need for contrast agents, can be used to monitor the acid–base imbalance triggered by the hypoxic TME. At $B_1=1 \mu\text{T}$ and $2 \mu\text{T}$, we observed a gradual increase in the MTR_{asym} value from Day 0 to Day 4 of treatment, followed by a gradual decline after Day 4 (Fig. 7B; Tables 2 and 3). The trend in the MTR_{asym} value was more pronounced at a lower field strength ($B_1=1 \mu\text{T}$), which indicates that a higher

field strength ($2 \mu\text{T}$) causes unwanted saturation effects, leading to an insignificant trend. Taken together, a 4-day imatinib regimen not only achieves antitumor effects and reduces high pericyte coverage but also decreases HIF-1 α expression, while prolonging the treatment leads to poor efficacy. Moreover, there was a negative correlation between the MTR_{asym} ($1 \mu\text{T}$) value and HIF-1 α expression, suggesting that the MTR_{asym} value at $1 \mu\text{T}$ can predict TME hypoxia and reflect HIF-1 α expression.

During the process of nontumor vascular maturation, PDGF-BB depletion leads to inadequate pericyte coverage, and increased Ang2 expression and TIE2 dissociation result in increased vessel leakage, inhibited maturation and severe hypoxia [13]. In tumors, increased Ang2 interferes with the binding of Ang1 to TIE2, thereby increasing tumor vessel permeability and inhibiting angiogenesis [80]. In our study, pericyte coverage was not only negatively correlated with vessel permeability and HIF-1 α expression but also strongly positively correlated with the MVD during imatinib treatment, which might suggest the existence of a similar mechanism in CRC. Thus, it remains to be experimentally validated whether the Ang1/TIE2 pathway is modulated by the imatinib-induced decrease in pericyte coverage, resulting in increased vessel permeability, inhibition of angiogenesis and exacerbation of later-stage hypoxia in high pericyte-coverage CRC. In addition, short-term imatinib treatment has been shown to improve oxygen delivery by reducing the IFP in CRC [73]. The initial decrease in HIF-1 α expression and increase in the MTR_{asym} ($1 \mu\text{T}$) value suggest that relief of early-stage hypoxia might be beneficial by decreasing the IFP. Moreover, nanodrugs loaded with Ang-2 siRNA inhibit angiogenesis and promote apoptosis via the Bcl-2/bax pathway in melanoma [81]. Our study also found that pericyte coverage was strongly positively correlated with the expression of Mcl-1, a component of the Bcl-2/bax pathway, during imatinib treatment. Considering the effectiveness of modulating Mcl-1 expression to reverse antitumor drug resistance, further experimental research is warranted to determine the role of the Ang1/TIE2 pathway and the Bcl-2/bax pathway in the effect of imatinib treatment.

Conclusion

In summary, we not only provided an effective imatinib regimen in high pericyte-coverage CRC, but also established an mpMRI system for monitoring the regulatory effect of imatinib on pericyte coverage and the TME. First, high pericyte coverage condition of CRC was decreased by imatinib and then reaching a plateau, accompanied by increased vessel permeability, decreased MVD, increased tumor apoptosis and 4-day decreased followed by restored HIF-1 α expression. Thus, we identified a 4-day imatinib regimen, concurrently achieves

effective antitumor efficacy, decreases pericyte coverage and HIF-1 α expression in the presence of high pericyte coverage. Moreover, we found that the DCE-derived V_e and K^{trans} values serve as representative imaging biomarkers for monitoring pericyte coverage during imatinib treatment and that the DWI-derived ADC value can be used to assess tumor proliferation and apoptosis. Additionally, the MTR_{asym} value at 1 μ T was found to have great value in monitoring hypoxia in the TME. This standardized evaluation system overcome the current challenge related to discontinuously observing changes in pericytes and TME during imatinib treatment.

Abbreviations

ADC	Apparent diffusion coefficient
ANOVA	One-way analysis of variance
APT CEST	Amide proton transfer chemical exchange saturation transfer
AUC	Area under the enhancement curve
CRC	Colorectal cancer
DCE	Dynamic contrast-enhanced
DMEM	Dulbecco's modified Eagle's medium
DWI	Diffusion-weighted imaging
ECM	Extracellular matrix
ECs	Endothelial cells
FOV	Field of view
HB-EGF	Heparin-binding EGF-like growth factor
HIF-1 α	Hypoxia inducible factor-1 α
IF	Immunofluorescence
IFP	Interstitial fluid pressure
LSD	Least significant difference
Mcl-1	Myeloid cell leukemia-1
MITK	Medical Imaging Interaction Toolkit
mpMRI	Multiparametric magnetic resonance imaging
MRS	Magnetic Resonance Spectroscopy
MVD	Microvessel density
NCCN	National Comprehensive Cancer Network
OCT	Optimal cutting temperature
PDGF-BB	Platelet-derived growth factor-BB
^{31}P	Phosphorous-31
qPCR	Quantitative polymerase chain reaction
TR	Repetition time
α -SMA	α -Smooth muscle actin
SDF-1 α	Stromal derived factor-1 α
9.4 T	9.4 Tesla
TE	Echo time
TME	Tumor microenvironment
T2WI	T2-weighted imaging
VIF	Vascular input function
VSMCs	Vascular smooth muscle cells

Supplementary Information

The online version contains supplementary material available at <https://doi.org/10.1186/s12967-024-05497-w>.

Supplementary Material 1

Supplementary Material 2

Acknowledgements

The authors thank the Animal Magnetic Resonance Research Center of the First Affiliated Hospital of Jinan University for providing technical support and MRI scanner (Bruker Biospec 9.4T).

Author contributions

MC, LL and CS contributed to design the study and revised the manuscript. XH contributed to conduct the experiments and draft the manuscript. KY

contributed to collect the imaging and pathological data; XH, KY, XZ, MM and JP contributed to data analysis. DZ, XZ, XM and XY revised it critically for important content. All authors have read and approved the manuscript.

Funding

This research was supported by the National Natural Science Foundation of China (No. 81971672, 82271943), the Guangzhou Science and Technology Plan Project (No. 2023A03J0609, 2023A03J1037, 202102010063), the Clinical Frontier Technology Program of the First Affiliated Hospital of Jinan University, China (No. JNU1AF-CFTP-2022-a01233), Guangzhou Basic Research Foundation (No. 202201020005), Guangdong Basic and Applied Basic Research Foundation (No. 2022A1515110630), Guangdong Medical Science and Technology Research Foundation (No. 20201124174036494), Scientific Research Program of Guangdong Provincial Bureau of Traditional Chinese Medicine (No. 20222039).

Data availability

The data and materials analyzed in this study can be accessed upon reasonable request to the corresponding author, subject to approval by the university's ethics committee.

Declarations

Ethics approval and consent to participate

All animal experiments were conducted in accordance with procedures approved by the Laboratory Animal Ethics Committee of Jinan University (No. 20220304-47).

Competing interests

All authors declared that they have no known competing financial interests or personal relationships that could have appeared to influence the work reported in this research.

Author details

¹Medical Imaging Center, The First Affiliated Hospital of Jinan University, West Huangpu Avenue No. 613, Guangzhou 510630, China

²Department of Medical Imaging, The Affiliated Guangdong Second Provincial General Hospital of Jinan University, Xingang Middle Road No. 466, Guangzhou 510317, China

³Engineering Research Center of Medical Imaging Artificial Intelligence for Precision Diagnosis and Treatment, West Huangpu Avenue No. 613, Guangzhou 510630, China

⁴Department of Radiology, Guangzhou First People's Hospital, Panfu Road No. 1, Guangzhou 510080, China

⁵Department of General Surgery, The First Affiliated Hospital of Jinan University, West Huangpu Avenue No. 613, Guangzhou 510630, China

⁶College of Pharmacy, Jinan University, West Huangpu Avenue No.601, Guangzhou 510632, China

Received: 10 April 2024 / Accepted: 10 July 2024

Published online: 31 July 2024

References

1. Siegel RL, Miller KD, Wagle NS, et al. Cancer statistics, 2023. *CA Cancer J Clin.* 2023;73(1):17–48.
2. Lopez A, Harada K, Vasilakopoulou M, et al. Target Angiogenesis Colorectal Carcinoma Drugs. 2019;79:63–74.
3. Benson AB, Venook AP, Al-Hawary MM, et al. Rectal Cancer, Version 2.2022, NCCN Clinical Practice guidelines in Oncology. *J Natl Compr Canc Netw.* 2022;20(10):1139–67.
4. Baeriswyl V, Christofori G. The angiogenic switch in carcinogenesis. *Semin Cancer Biol.* 2009;19(5):329–37.
5. Grothey A, Van Cutsem E, Sobrero A, et al. Regorafenib monotherapy for previously treated metastatic colorectal cancer (CORRECT): an international, multicentre, randomised, placebo-controlled, phase 3 trial. *Lancet.* 2013;381(9863):303–12.
6. Bennouna J, Sastre J, Arnold D, et al. Continuation of bevacizumab after first progression in metastatic colorectal cancer (ML18147): a randomised phase 3 trial. *Lancet Oncol.* 2013;14(1):29–37.

7. Jiang Z, Zhou J, Li L, et al. Pericytes in the tumor microenvironment. *Cancer Lett.* 2023;556:216074.
8. Gerhardt H, Betsholtz C. Endothelial-pericyte interactions in angiogenesis. *Cell Tissue Res.* 2023;314(1):15–23.
9. Armulik A, Genove G, Betsholtz C. Pericytes: developmental, physiological, and pathological perspectives, problems, and promises. *Dev Cell.* 2011;21(2):193–215.
10. Hellstrom M, Gerhardt H, Kalen M, et al. Lack of pericytes leads to endothelial hyperplasia and abnormal vascular morphogenesis. *J Cell Biol.* 2001;153(3):543–53.
11. Villaseñor R, Kuennecke B, Ozmen L, et al. Region-specific permeability of the blood-brain barrier upon pericyte loss. *J Cereb Blood Flow Metab.* 2017;37(12):3683–94.
12. Pallone TL, Silldorff EP. Pericyte regulation of renal medullary blood flow. *Exp Nephrol.* 2001;9(3):165–70.
13. Park DY, Lee J, Kim J, et al. Plastic roles of pericytes in the blood-retinal barrier. *Nat Commun.* 2017;8:15296.
14. Moench R, Gasser M, Nawalaniec K, et al. Platelet-derived growth factor (PDGF) cross-signaling via non-corresponding receptors indicates bypassed signaling in colorectal cancer. *Oncotarget.* 2022;19(13):1140–52.
15. Zhou L, Sun X, Huang Z, et al. Imatinib ameliorated retinal neovascularization by suppressing PDGFR-alpha and PDGFR-beta. *Cell Physiol Biochem.* 2018;48(1):263–73.
16. Gergely PA, Murnyak B, Bencze J, et al. Tyrosine kinase inhibitor Imatinib Mesylate alters DMBA-Induced early Onco/Suppressor gene expression with tissue-specificity in mice. *Biomed Res Int.* 2019;2019:8670398.
17. Cooke VG, LeBleu VS, Keskin D, et al. Pericyte depletion results in hypoxia-associated epithelial-to-mesenchymal transition and metastasis mediated by met signaling pathway. *Cancer Cell.* 2012;21(1):66–81.
18. Tsao AS, Liu S, Fujimoto J, et al. Phase II trials of imatinib mesylate and docetaxel in patients with metastatic non-small cell lung cancer and head and neck squamous cell carcinoma. *J Thorac Oncol.* 2011;6(12):2104–11.
19. Kerob D, Porcher R, Verola O, et al. Imatinib mesylate as a preoperative therapy in dermatofibrosarcoma: results of a multicenter phase II study on 25 patients. *Clin Cancer Res.* 2010;16(12):3288–95.
20. Safra T, Andreopoulou E, Levinson B, et al. Weekly paclitaxel with intermittent imatinib mesylate (gleevec): tolerance and activity in recurrent epithelial ovarian cancer. *Anticancer Res.* 2010;30(9):3243–7.
21. Caspani EM, Crossley PH, Redondo-Garcia C, et al. Glioblastoma: a pathogenic crosstalk between tumor cells and pericytes. *PLoS ONE.* 2014;9(7):e101402.
22. Yang Y, Andersson P, Hosaka K, et al. The PDGF-BB-SOX7 axis-modulated IL-33 in pericytes and stromal cells promotes metastasis through tumour-associated macrophages. *Nat Commun.* 2016;7:11385.
23. Bose A, Barik S, Banerjee S, et al. Tumor-derived vascular pericytes anergize th cells. *J Immunol.* 2013;191(2):971–81.
24. Nolan-Stevaux O, Truitt MC, Pahler JC, et al. Differential contribution to neuroendocrine tumorigenesis of parallel egfr signaling in cancer cells and pericytes. *Genes Cancer.* 2010;1(2):125–41.
25. Mancuso MR, Davis R, Norberg SM, et al. Rapid vascular regrowth in tumors after reversal of VEGF inhibition. *J Clin Invest.* 2006;116(10):2610–21.
26. Huang M, Chen M, Qi M, et al. Perivascular cell-derived extracellular vesicles stimulate colorectal cancer revascularization after withdrawal of antiangiogenic drugs. *J Extracell Vesicles.* 2021;10(7):e12096.
27. Abdullah SE, Perez-Soler R. Mechanisms of resistance to vascular endothelial growth factor blockade. *Cancer.* 2012;118(14):3455–67.
28. Chen M, Lei X, Shi C, et al. Pericyte-targeting prodrug overcomes tumor resistance to vascular disrupting agents. *J Clin Invest.* 2017;127(10):3689–701.
29. Bergers G, Hanahan D. Modes of resistance to anti-angiogenic therapy. *Nat Rev Cancer.* 2008;8(8):592–603.
30. Bergers G, Song S. The role of pericytes in blood-vessel formation and maintenance. *Neuro Oncol.* 2005;7(4):452–64.
31. Chrastina A, Massey KA, Schnitzer JE. Overcoming in vivo barriers to targeted nanodelivery. *Wiley Interdiscip Rev Nanomed Nanobiotechnol.* 2011;3(4):421–37.
32. Kano MR, Komuta Y, Iwata C, et al. Comparison of the effects of the kinase inhibitors imatinib, sorafenib, and transforming growth factor-beta receptor inhibitor on extravasation of nanoparticles from neovasculature. *Cancer Sci.* 2009;100(1):173–80.
33. Zhang L, Nishihara H, Kano MR. Pericyte-coverage of human tumor vasculature and nanoparticle permeability. *Biol Pharm Bull.* 2012;35(5):761–6.
34. Guo P, Hu B, Gu W, et al. Platelet-derived growth factor-B enhances glioma angiogenesis by stimulating vascular endothelial growth factor expression in tumor endothelia and by promoting pericyte recruitment. *Am J Pathol.* 2003;162(4):1083–93.
35. Furuhashi M, Sjoblom T, Abramsson A, et al. Platelet-derived growth factor production by B16 melanoma cells leads to increased pericyte abundance in tumors and an associated increase in tumor growth rate. *Cancer Res.* 2004;64(8):2725–33.
36. Keskin D, Kim J, Cooke VG, et al. Targeting vascular pericytes in hypoxic tumors increases lung metastasis via angiopoietin-2. *Cell Rep.* 2015;10(7):1066–81.
37. Beroukhi R, Mermel CH, Porter D, et al. The landscape of somatic copy-number alteration across human cancers. *Nature.* 2010;463(7283):899–905.
38. Krajewski S, Bodrug S, Krajewska M, et al. Immunohistochemical analysis of Mcl-1 protein in human tissues. Differential regulation of Mcl-1 and Bcl-2 protein production suggests a unique role for Mcl-1 in control of programmed cell death in vivo. *Am J Pathol.* 1995;146(6):1309–19.
39. Song X, Shen L, Tong J, et al. Mcl-1 inhibition overcomes intrinsic and acquired regorafenib resistance in colorectal cancer. *Theranostics.* 2020;10(18):8098–110.
40. Kelly PN, Strasser A. The role of Bcl-2 and its pro-survival relatives in tumorigenesis and cancer therapy. *Cell Death Differ.* 2011;18(9):1414–24.
41. Percivalle RM, Opferman JT. Delving deeper: MCL-1's contributions to normal and cancer biology. *Trends Cell Biol.* 2013;23(1):22–9.
42. Franco M, Roswall P, Cortez E, et al. Pericytes promote endothelial cell survival through induction of autocrine VEGF-A signaling and Bcl-w expression. *Blood.* 2011;118(10):2906–17.
43. Shi C, Liu D, Xiao Z, et al. Monitoring tumor response to Antivascular Therapy using Non-contrast Intravoxel Incoherent Motion Diffusion-Weighted MRI. *Cancer Res.* 2017;77(13):3491–501.
44. Liang J, Cheng Q, Huang J, et al. Monitoring tumour microenvironment changes during anti-angiogenesis therapy using functional MRI. *Angiogenesis.* 2019;22(3):457–70.
45. Zhou H, Chen M, Zhao D. Longitudinal MRI evaluation of intracranial development and vascular characteristics of breast cancer brain metastases in a mouse model. *PLoS ONE.* 2013;8(4):e62238.
46. O'Connor JP, Rose CJ, Waterton JC, et al. Imaging intratumor heterogeneity: role in therapy response, resistance, and clinical outcome. *Clin Cancer Res.* 2015;21(2):249–57.
47. O'Connor JP, Jackson A, Asselin MC, et al. Quantitative imaging biomarkers in the clinical development of targeted therapeutics: current and future perspectives. *Lancet Oncol.* 2008;9(8):766–76.
48. Padhani AR, Liu G, Koh DM, et al. Diffusion-weighted magnetic resonance imaging as a cancer biomarker: consensus and recommendations. *Neoplasia.* 2009;11:102–25.
49. Lei X, Chen M, Huang M, et al. Desacetylvinblastine Monohydrate disrupts Tumor vessels by promoting VE-cadherin internalization. *Theranostics.* 2018;8(2):384–98.
50. Hayashida Y, Yakushiji T, Awai K, et al. Monitoring therapeutic responses of primary bone tumors by diffusion-weighted image: initial results. *Eur Radiol.* 2006;16(12):2637–43.
51. Ng TC, Majors AW, Vijayakumar S, et al. Human neoplasm pH and response to radiation therapy: P-31 MR spectroscopy studies in situ. *Radiology.* 1989;170(3):875–8.
52. Petroff OA, Prichard JW, Behar KL, et al. Cerebral intracellular pH by 31P nuclear magnetic resonance spectroscopy. *Neurology.* 1985;35(6):781–8.
53. Zhou J, Payen JF, Wilson DA, et al. Using the amide proton signals of intracellular proteins and peptides to detect pH effects in MRI. *Nat Med.* 2003;9(8):1085–90.
54. Krikken E, van der Kemp WJM, Khlebnikov V, et al. Contradiction between amide-CEST signal and pH in breast cancer explained with metabolic MRI. *NMR Biomed.* 2019;32(8):e4110.
55. Paech D, Dreher C, Regnery S, et al. Relaxation-compensated amide proton transfer (APT) MRI signal intensity is associated with survival and progression in high-grade glioma patients. *Eur Radiol.* 2019;29(9):4957–67.
56. Vohra R, Wang YN, Son H, et al. Non-invasive monitoring of increased fibrotic tissue and Hyaluronan Deposition in the Tumor Microenvironment in the Advanced stages of pancreatic ductal adenocarcinoma. *Cancers (Basel).* 2022;14(4):999.
57. Ruan J, Luo M, Wang C, et al. Imatinib disrupts lymphoma angiogenesis by targeting vascular pericytes. *Blood.* 2013;121(26):5192–202.
58. Shrivastav S, Bal A, Singh G, et al. Tumor angiogenesis in breast Cancer: Pericytes and Maturation does not correlate with Lymph Node Metastasis and Molecular subtypes. *Clin Breast Cancer.* 2016;16(2):131–8.

59. Li W, Zhao X, Du B, et al. Gold nanoparticle-mediated targeted delivery of recombinant human endostatin normalizes Tumour vasculature and improves Cancer Therapy. *Sci Rep*. 2016;6:30619.
60. Nolden M, Zelzer S, Seitel A, et al. The Medical Imaging Interaction Toolkit: challenges and advances: 10 years of open-source development. *Int J Comput Assist Radiol Surg*. 2013;8(4):607–20.
61. Tofts PS, Brix G, Buckley DL, et al. Estimating kinetic parameters from dynamic contrast-enhanced T (1)-weighted MRI of a diffusible tracer: standardized quantities and symbols. *J Magn Reson Imaging*. 1999;10(3):223–32.
62. Loveless ME, Halliday J, Liess C, et al. A quantitative comparison of the influence of individual versus population-derived vascular input functions on dynamic contrast enhanced-MRI in small animals. *Magn Reson Med*. 2012;67(1):226–36.
63. Park H, Kim SH, Kim JY. Dynamic contrast-enhanced magnetic resonance imaging for risk stratification in patients with prostate cancer. *Quant Imaging Med Surg*. 2022;12(1):742–51.
64. De Bruyne S, Van Damme N, Smeets P, et al. Value of DCE-MRI and FDG-PET/CT in the prediction of response to preoperative chemotherapy with bevacizumab for colorectal liver metastases. *Br J Cancer*. 2012;106(12):1926–33.
65. Guivel-Scharen V, Sinnwell T, Wolff SD, et al. Detection of proton chemical exchange between metabolites and water in biological tissues. *J Magn Reson*. 1998;133(1):36–45.
66. Zaiss M, Schmitt B, Bachert P. Quantitative separation of CEST effect from magnetization transfer and spillover effects by Lorentzian-line-fit analysis of z-spectra. *J Magn Reson*. 2011;211(2):149–55.
67. Ferland-McCollough D, Slater S, Richard J, et al. Pericytes, an overlooked player in vascular pathobiology. *Pharmacol Ther*. 2017;171:30–42. <https://doi.org/10.1016/j.pharmthera.2016.11.008>.
68. Meng MB, Zaorsky NG, Deng L, et al. Pericytes: a double-edged sword in cancer therapy. *Future Oncol*. 2015;11(1):169–79.
69. Iqbal N. Iqbal N. Imatinib: a breakthrough of targeted therapy in cancer. *Chemother Res Pract*. 2014;2014:357027.
70. Kim J. Pericytes in breast Cancer. *Adv Exp Med Biol*. 2019;1147:93–107.
71. Cao Y, Zhang ZL, Zhou M, et al. Pericyte coverage of differentiated vessels inside tumor vasculature is an independent unfavorable prognostic factor for patients with clear cell renal cell carcinoma. *Cancer*. 2013;119(2):313–24.
72. Zhou W, Chen C, Shi Y, et al. Targeting glioma stem cell-derived Pericytes disrupts the blood-tumor barrier and improves chemotherapeutic efficacy. *Cell Stem Cell*. 2017;21(5):591–e603594.
73. Burmakin M, van Wieringen T, Olsson PO, et al. Imatinib increases oxygen delivery in extracellular matrix-rich but not in matrix-poor experimental carcinoma. *J Transl Med*. 2017;15(1):47.
74. Abramsson A, Lindblom P, Betsholtz C. Endothelial and nonendothelial sources of PDGF-B regulate pericyte recruitment and influence vascular pattern formation in tumors. *J Clin Invest*. 2003;112(8):1142–51.
75. Stratman AN, Schwindt AE, Malotte KM, et al. Endothelial-derived PDGF-BB and HB-EGF coordinately regulate pericyte recruitment during vasculogenic tube assembly and stabilization. *Blood*. 2010;116(22):4720–30.
76. Stratman AN, Davis MJ, Davis GE. VEGF and FGF prime vascular tube morphogenesis and sprouting directed by hematopoietic stem cell cytokines. *Blood*. 2011;117(14):3709–19.
77. Lindgren A, Anttila M, Arponen O, et al. Dynamic contrast-enhanced MRI to characterize angiogenesis in primary epithelial ovarian cancer: an exploratory study. *Eur J Radiol*. 2023;165:110925.
78. Backus HH, Van Groeningen CJ, Vos W, et al. Differential expression of cell cycle and apoptosis related proteins in colorectal mucosa, primary colon tumours, and liver metastases. *J Clin Pathol*. 2002;55(3):206–11.
79. Ioannou M, Paraskeva E, Baxeivanidou K, et al. HIF-1alpha in colorectal carcinoma: review of the literature. *J BUON*. 2015;20(3):680–9.
80. Duran CL, Borriello L, Karagiannis GS, et al. Targeting Tie2 in the Tumor Microenvironment: from angiogenesis to dissemination. *Cancers (Basel)*. 2021;13(22):13225730.
81. Shan X, Yu W, Ni X, et al. Effect of Chitosan magnetic nanoparticles loaded with Ang2-siRNA plasmids on the growth of Melanoma xenografts in Nude mice. *Cancer Manag Res*. 2020;12:7475–85.

Publisher's Note

Springer Nature remains neutral with regard to jurisdictional claims in published maps and institutional affiliations.